Jakob Ruttinger, BSc

Vehicle Dynamics Optimization using Performance Envelope for Steer-by-Torque-Vectoring Application

Master's Thesis

to achieve the university degree of Diplom-Ingenieur in the master's degree program of Mechanical Engineering and Business Economics

submitted to

Graz University of Technology

Supervisor

Dipl. -Ing. Andreas Hackl, BSc
Institute of Automotive Engineering

Dipl. -Ing. Dr. techn. Carlo Miano
ThyssenKrupp Presta AG

Graz, October 2017

Restricted access until October 2022

Danksagung

Ich möchte mich bei allen Parteien, die zum Zustandekommen dieser Arbeit beigetragen haben herzlich bedanken.

Beginnend danke ich dem Institut für Fahrzeugtechnik der TU Graz für die Initiierung dieser interessanten Masterarbeit. Besonders möchte ich mich bei meinem Betreuer Andreas Hackl bedanken, der als treibende Kraft die Kooperation mit der Firma ThyssenKrupp Presta möglich gemacht hat, und mir immer mit seinem Fachwissen unterstützend zur Seite stand. Weiters danke ich Cornelia Lex und Professor Arno Eichberger für deren konstruktiven Input zur Finalisierung der schriftlichen Arbeit.

Ich möchte mich auch bei der ganzen Abteilung für Innovation und Technik der Kooperationsfirma bedanken für eine sehr lehrreiche und interessante Zeit in Liechtenstein. Ganz besonders bedanke ich mich bei meinem Mentor Carlo Miano, dessen Ideen stets inspirierend waren und fundamental zu den Ergebnissen der Arbeit beigetragen haben.

Ein großer Dank gilt auch Professor Georg Rill der das, der Arbeit zugrundeliegende Fahrzugmodell, zur Verfügung gestellt hat.

Ein besonderer Dank gilt meiner Familie die mich immer unterstütz hat und meinen Freunden für die schöne gemeinsame Studienzeit.

Abschließend möchte ich meiner Freundin danken, die mir stets stärkend zur Seite stand.

Statutory Declaration

I declare that I have authored this thesis independently, that I have not used other than the declared sources / resources, and that I have explicitly marked all material which has been quoted either literally or by content from the used sources.

date (signature)

Eidesstattliche Erklärung

Ich erkläre an Eides statt, dass ich die vorliegende Arbeit selbstständig verfasst, andere als die angegebenen Quellen/Hilfsmittel nicht benutzt, und die den benutzten Quellen wörtlich und inhaltlich entnommenen Stellen als solche kenntlich gemacht habe.

Datum (Unterschrift)

Abstract

Following the trends observed in the automobile industry, novel steering systems, based on the "by-wire" technology, are investigated in this thesis. In particular steering by torque vectoring is examined. Therefore, a computation methodology in MATLAB is developed to calculate ratings for vehicle dynamics. Further the effects are studied on a specifically modified BMW X5, provided by the company Thyssenkrupp Presta AG.

The basis of the methodology is formed by a multi-body vehicle model developed by Professor Georg Rill. This model has been adapted, parametrized and validated in preceding works and tailored to the testing vehicle.

As representative value for vehicle performance the area of the performance envelope is introduced and declared as performance index. It quantifies the potential of the achievable horizontal forces acting on the car. Additionally, the vehicle behavior is classified and a method to calculate the stability is shown.

The performance envelope and the vehicle behavior are computed point-wise using a constraint optimization technique. For each point equations, representing a quasi-steady-state vehicle condition are derived and used as constraints.

Due to the performance loss caused by the application of the steer-by-torque vectoring compared to the steer-by-wire system, a vehicle parameter analysis is carried out. The caster trail and the king pin offset are identified as the geometric dimensions with the highest impact on vehicle performance. Further adjusting the roll-balance emerges as possible potential to regain performance.

By a modification of the steering geometry of the test vehicle according to the insights gathered, the expected performance gain is proven. The optimum values are computed in a parameter optimization, and a huge improvement is shown.

Zusammenfassung

Diese Arbeit beschäftigt sich mit neuartigen Lenksystemen, basierend auf Idee Räder und Lenkrad mechanisch zu trennen. Im Speziellen wird das Lenken durch Aufbringen von unterschiedlichen Antriebsmomenten untersucht. Es wird dazu eine Berechnungsmethode in MATLAB entwickelt, die Fahrzeuge mit solchen Lenksystemen objektiv bewerten soll. Ein spezielles Testfahrzeug wird von der Firma ThyssenKrupp Presta zur Verfügung gestellt um die Berechnungsergebnisse validieren zu können.

Die Berechnungsmethodik basiert auf einem Mehrkörper-Simulationsmodell, dass von Professor Georg Rill entwickelt wurde. Dieses Modell wurde in vorangegangen Arbeiten adaptiert und mit dem Testfahrzeug validiert.

Zur Fahrzeugbewertung wird der Performance Index definiert. Er ergibt sich aus der Fläche unter der Kurve die das Potenzial der auf das Fahrzeug wirkenden horizontalen Kräfte beschreibt. Weiters wird gezeigt, dass auch die Bewertung des Fahrverhalten auf einen Wert reduziert werden kann und zu Stabilitäts-Untersuchungen herangezogen werden kann.

Die Berechnung von Fahrzeug Performance und Fahrverhalten erfolgt punktweise. Jeder Punkt entspricht dabei einem quasi-stationärem Fahrzeugzustand. Alle, zur Beschreibung dieses Zustandes notwendigen Gleichungen werden hergeleitet und in einem Optimierungsverfahren als Zusatzbedingungen formuliert.

Im nächsten Schritt wird gezeigt, dass die Verwendung des beschriebenen Lenksystems zu einer erheblichen Verschlechterung der Fahrzeugperformance, im Vergleich zur herkömmlichen Lenkung, führt. Die Fahrwerksparameter werden analysiert und der Störkrafthebelarm und der Nachlauf werden als einflussreichste Größen identifiziert. Auch in der Anpassung der Rollsteifigkeiten wird als Potential gesehen die Performance wieder zu verbessern.

Zuletzt wird anhand von Tests mit dem Fahrzeug gezeigt, dass es möglich ist, durch leichte Veränderungen am Fahrwerk, die Fahrzeugperformance stark zu verbessern.

Contents

Abbreviations

acc	Acceleration
arb/ARB	Anti-roll bar
brk	Braking
crit	Critical
CoG	Center of gravity
des	Desired
ESC	Electronic stability control
kph	Kilometers per hour
lat	Lateral
max	Maximum
min	Minimum
SbTV	Steer-by-torque vectoring
SbW	Steer-by-wire
TV	Torque vectoring
vrt	vertical
w	Wheel
WT	Weight transfer
2D	Two-dimensional
3D	Three-dimensional

Symbols

In this thesis, no separate notation of scalars, vectors and matrices is used.

General Notation

The appearance of dots, sub- and superscripts in context with the used variables is explained below, where the letters a to d represent the position of the optional assignments.

$\dot{x}_{\mathrm{ab,c}}(\mathrm{d})$

a	Initial position of vector
b	End position of vector
c	Reference coordinate system
d	Shows the parameters vector x is depending on
$\dot{x}$	Time derivative of vector x
$\ddot{x}$	Second order time derivative of vector x

Parameters

$a_{0i,0}$	Vector of acceleration of the body i
$A_{\mathrm{0F,0}}$	Rotation matrix of the vehicle fixed axis system in respect to the earth-fixed system
a_x	Vehicle acceleration in x-direction
a_y	Vehicle acceleration in y-direction
a_z	Vehicle acceleration in z-direction
C_{f}	Roll stiffness of front axle
C_{r}	Roll stiffness of rear axle
d_{iu}	Partial derivation of the wheelcenter rotation to the rack position
F_{fr}	Stick slip friction force on steering rack
$F_{i,0}$	Vector of total force of body i
$F_{i,0}^{\mathrm{a}}$	Vector of all but constraint forces of body i
$F_{i,0}^{\mathrm{c}}$	Vector of constraint forces of body i
$F_{i,C}$	Vector of tire force in the wheel center i

F_z	Vertical tire load
h_{CoG}	Distance from center of gravity to the ground
l	Wheelbase
m_i	Mass of body i
M	Mass matrix of vehicle
M_{acc}	Torque around king pin axle caused by acceleration force
MB	Mechanical vehicle balance
M_{brk}	Torque around king pin axle caused by braking force
$M_{\mathrm{r},i}$	Torque around king pin axle caused by steering rack force
M_{vrt}	Torque around king pin axle caused by vertical tire force
M_u	Reduced masses to the steering rack
M_z	Aligning torque of the wheel
PI	Performance index
$r_{0\mathrm{F},0}$	Position of the vehicle fixed axis system in respect to the earth-fixed system
$r_{0i,0}$	Position of the wheel center of wheel i in respect to the earth fixed axis system
r_{a}	King pin offset
$r_{\mathrm{D},i}$	Dynamic tire radius of wheel i
$r_{\mathrm{F}i,\mathrm{F}}$	Position of the wheel center of wheel i in respect to the vehicle fixed axis system
r_{P}	Caster trail
R	Instant corner radius
$s_{x,i}$	Longitudinal tire slip on tire i
SI	Steering index
t_{iu}	Partial derivation of the wheelcenter position to the rack position
$T_{i,0}$	Vector of total torque of body i
$T_{i,0}^{\mathrm{a}}$	Vector of all but constraint torques of body i
$T_{i,0}^{\mathrm{c}}$	Vector of constraint torques of body i
$T_{i,C}$	Vector of tire torque in the wheel center i
u	Steering rack position

u_{arb}	Deflection of anti-roll bar
u_{d}	Damper movement
u_{front}	Rack position on the front axle
u_{rear}	Rack position on the rear axle
u_{s}	Spring movement
v	Vector of vehicle velocity
x	Vector of generalized coordinates and generalized velocities
y	Vector of generalized coordinates
z	Vector of generalized velocities
z_i	Suspension movement of suspension i
α	Roll angle
$\alpha_{0i,0}$	Vector of the angular acceleration of body i
α_{f}	Sideslip angle on front axle
α_i	Sideslip angle of wheel i
α_{r}	Sideslip angle on rear axle
β	Pitch angle
γ	Yaw angle
δ_u	Friction coefficient of steering rack bearing
$\delta v_{0i,0}$	Vector of virtual velocity of body i
$\delta\omega_{0i,0}$	Vector of virtual angular velocity of body i
$\theta_{i,0}$	Tensor of moments of inertia of body i
μ	Road friction coefficient
σ	King pin inclination
τ	Caster angle
φ_i	Generalized coordinate of suspension i
$\omega_{0i,0}$	Vector of the angular velocity of body i
Ω_i	Angular velocity of wheel i

1 Introduction

1.1 ThyssenKrupp Presta AG

ThyssenKrupp Presta (TKP) is one of the world leading steering manufacturer with its headquarters located in Eschen in Liechtenstein [1]. Specialized in cold forging of steering parts, the company is a supplier to many well-known automotive manufacturers.

TKP has 7000 employees worldwide and around 2000 are working in Liechtenstein. The company is a subsidiary of the ThyssenKrupp group and part of the "Components Technology" business area.

Beside manufacturing of ordinary steering-systems and several types of electromechanically power assisted steering systems (EPAS), TKP is conducting research in the field of steer-by-wire (SbW) systems and other advanced steering methods.

1.2 Steering System Development

Around the early 1980's Rudolph Ackermann invented a steering system, where each wheel is moved separately. In a corner, the inner wheel has a higher wheel steering angle to reduce tire wear. This is achieved by a system of knuckles and angled steering arms [2].

Specific parameters of the so-called steering geometry describe the dimensions and arrangement of these elements and define the steering motion of the wheels. Further, the amount and behavior of the feedback forces induced by the wheels are influenced by the geometry of steering system.

In the last decades, this system has been actuated by a steering gear connected to the steering wheel by a shaft. The forces acting on the wheels were transmitted directly to the driver via this pure mechanical system and resulted in a huge steering effort. Therefore, passive steering assistant systems were introduced, to support the driver by generating an additional steering torque. One representative of these systems is the rack-EPAS, where an electrical motor is located at the steering rack. This technology is fundamental for new approaches of decoupling steering wheel and steering gear the so-called steer-by-wire (SbW) systems.

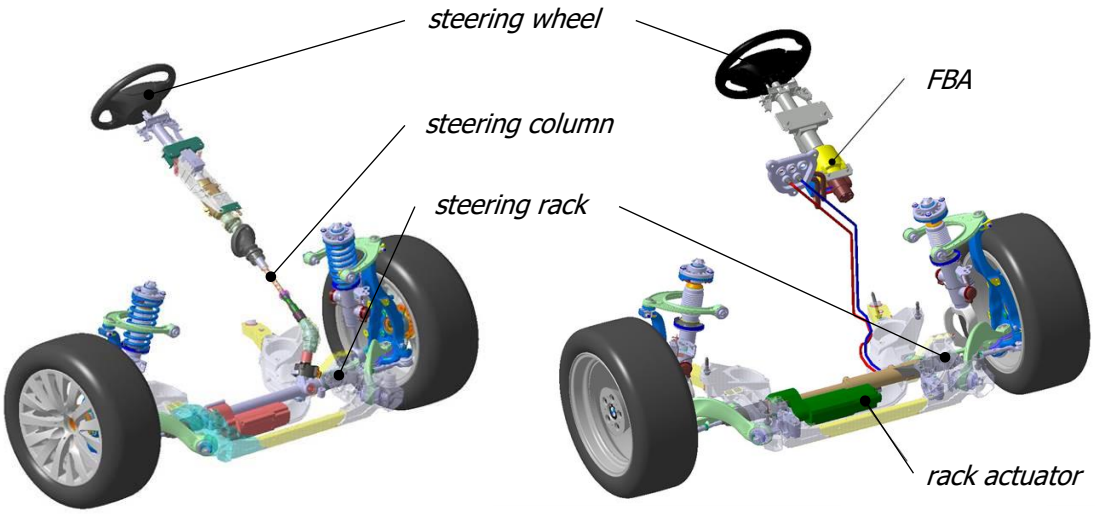

(a) EPAS (b) SbW

Figure 1.1: Components of EPAS and SbW steering systems [3]

In Figure 1.1 is shown that the EPAS system depicted in (a) can be adapted to the SbW system (b) by removing the steering column and adding a feedback actuator (FBA) unit. As the electrical rack actuator is not used to just support the steering force, but generating the whole rack force by its own, it has to be replaced with a more powerful unit.

1.2.1 Steer-by-Wire (SbW)

SbW systems have no mechanical connection between steering wheel and the steered wheels. That means the steering input, given by the driver is transmitted electrically to a steering actuator to turn the tires. In reverse, the feedback forces are determined and passed to the driver via a FBA located near the steering wheel. Depicted in Figure 1.1 (b) is the basic structure of a SbW System. Table 1-1 gives an overview of some of the positive and the negative aspects of this steering system.

Table 1-1: Advantages and disadvantages of a SbW system based on [4]

Advantages	Disadvantages
+ High functionality (dynamic steering ration, vehicle stabilization, …)	– Higher costs because of redundancy requirements
+ Packaging	– Complexity
+ Increased passive vehicle safety (no steering column)	– Higher weight
+ Simplification of the steering geometry	
+ Increased active vehicle safety (driving assistance system)	
+ Easy tuning of driver feedback	

1.2.2 Steer-by-Torque Vectoring (SbTV)

For the vast majority of the road vehicles it is desired that after a steering input of the driver the steering wheel tends to rotate back to the neutral position by its own. This means the steering has to be self-aligning. This property is realized by a certain suspension geometry and steering design [5].

Depicted in Figure 1.2 is a simplified model of a steered front axle. A more detailed 3D model will be discussed in 7.2. The sketch gives an overview of the acting forces and the geometric dimensions with influence on the steering forces. During steering the wheel i is rotated around point A_i. In this thesis only steering systems with a common steering rack are investigated. For a SbW system it is not mandatory to connect the steered wheels with each other.

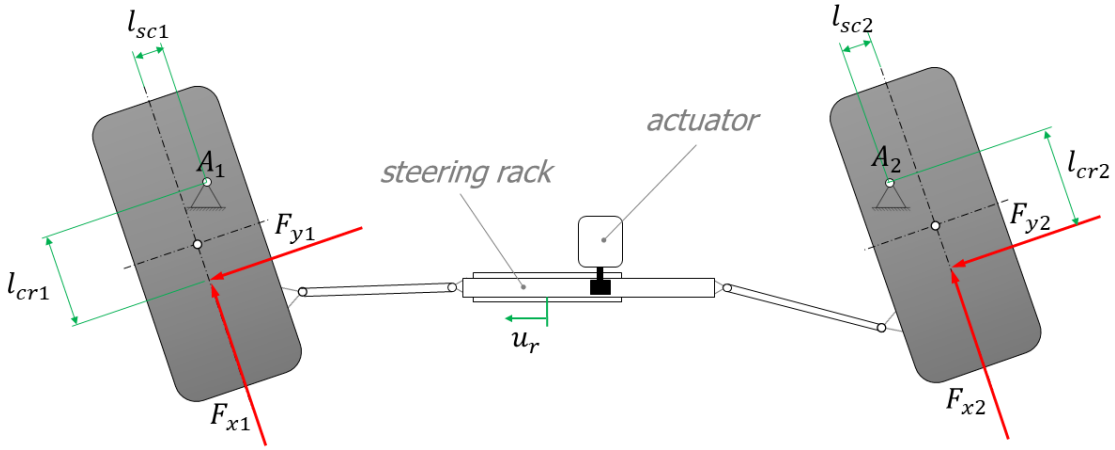

Figure 1.2: Effects on steering alignment

Generally, the induced steering torque of the wheels is mainly affected by the lateral forces F_{y1} and F_{y2} and by the levers l_{cr1} and l_{cr2}. For conventional vehicles, the lateral offsets of the longitudinal tire forces l_{sc1} and l_{sc2} are tried to be minimized, to reduce steering torques induced by selective braking in case of an interfering ESC system [5]. For the performance of a SbTV system these are the most influencing dimensions as they are also causing a certain amount of steering torque induced by the driving torques.

Typically, a vehicle equipped with one or more power units, applies the same torque to the left and to the right wheel on every driven axle if a conventional differential is used. The driving torques induce longitudinal tire forces which affect the speed and the longitudinal acceleration of the vehicle. Torque vectoring refers to the ability of applying different torques to the wheels.

If different driving torques are applied to the left and the right wheel of the steered axle, the resulting unequal longitudinal tire forces induce different steering torques and force the car to steer. Additionally, a torque around the vertical vehicle axis is imposed.

The torque distribution either can be done using

- torque vectoring differentials,
- independent driving units,
- or a brake by wire (BbW) system [6].

In this thesis only front-wheel-drive (FWD) vehicles powered with two independent electrical motors and front-wheel steering are investigated, but SbTV on the rear axle is also conceivable.

1.3 Motivation

According to [7], two major trends in the automotive industry related to steering systems can be observed. Autonomous driving and SbW. Because no moving steering wheel is wanted in an autonomous driven car, the SbW system is also a fundamental part of it. A major safety issue comes along with the fact of having no mechanical connection from the steering wheel to the steering rack. Consequently, it is necessary to develop fallback mechanisms and redundant SbW systems.

With the rising interest in electric vehicles, the industry starts to exploit the benefits of using more than one power units. Thus, realization of torque vectoring systems is no longer depending on expensive and complex differential units.

In a vehicle, capable of controlling the amount of torque applied to the wheels on the steered axle, the SbTV system could be used as fallback level for the SbW or the EPAS system [7], or even as complete replacement to reduce overall costs and weight.

Another possible application area is the support of electronic EPAS and SbW systems, to reduce the energy demand [8]. In [9] it is shown that TV used instead of conventional power assisted steering systems can reduce the steering effort of the driver significantly.

The effectivity of the SbTV system is highly depending on the steering kinematic. As mentioned before, a conventional steering geometry is designed with the objective of returning the steered wheels back into the straight-line position because of the good drivability. But with the possibility to control the position of the wheels and the feedback given to the driver independently, new perspectives open up. As no attempt in literature can be found of using SbTV exclusively as steering system, the focus of this thesis is to investigate this opportunity of steering and to develop a methodology to rate the vehicle performance.

Generally, the intention of the engineers is to keep the steering torques, induced by the longitudinal tire forces, low. This is done to reduce the steering effects, when ESP system engages. Because of this, it is expected that there will be a performance loss under the use of pure SbTV in a vehicle with unchanged steering geometry.

1.4 Objective

The main task of this thesis is, to set up an optimization algorithm, to find a set of suspension parameters with the best utilization of the SbTV system for a specific vehicle. The principles of an optimization process are shown in Figure 1.3.

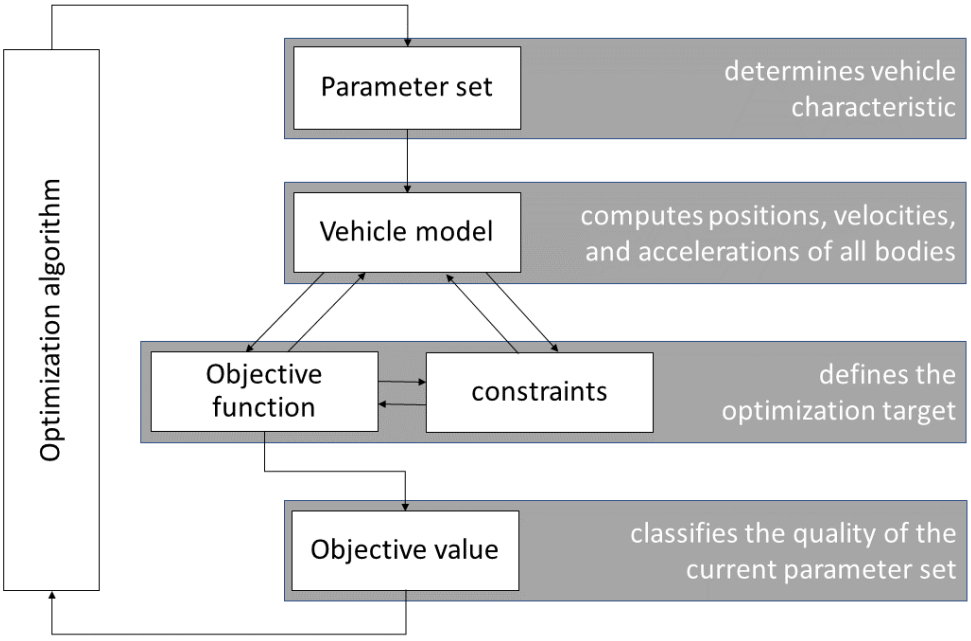

Figure 1.3: Optimization process

The objective function consisting of functions and variables, formulates the optimization criterion. The algorithm tries to minimize or maximize the objective value, the so called optimum, by changing the optimization parameter. The constraints are a set of equations and inequations and represent restrictions for the optimization parameters [10]. In the field of numerical optimization problems, there are two main strategies to find the best combination of parameters:

- deterministic optimization methods
- and stochastic optimization methods [11].

With the objective function, the objective value is computed with respect to the given constraints. This value has to be a measure of the vehicle performance and sensitive to changes of vehicle parameters.

1.5 Test Vehicle

To substantiate the theoretical investigation of the SbTV system, a research vehicle is taken as reference. The basis of this vehicle is a BMW X5 e70 2007 model depicted in Figure 1.4. This BMW X5 was modified by a group of students from the ETH Zurich as part of the research project SUNCAR [12]. The combustion engine has been removed as well as the driveshaft to the rear axle and replaced by two electric motors in the front, each powering one wheel.

Figure 1.4: Test vehicle BMW X5 e70 [12]

The conventional steering system has been adapted for a SbW system. With a clutch in the steering column it is possible to couple and decouple the mechanical connection of the steering wheel with the steering gear at any time. Because of the individually driven front wheels the car can also be operated in the SbTV mode.

The vehicle is equipped with additional sensors and measurement systems, to collect reference data for the validation of the vehicle model. Basic information about the vehicle can be found in Table 1-2.

Table 1-2: Specification sheet of testing vehicle

Engine	
Type	2 × Brusa HSM1-10.18.13
Power	2 × 84 kW
Torque	2 × 305 Nm
Gear box	
Type	Single speed
Transmission ratio	1: 5.5
Dimensions	
Wheel base	2.933 m
Front track wide	1.644 m
Rear track wide	1.650 m
Vehicle weight	2843 kg
Suspension	
Front	Four-link
Rear	Integral IV

2 Vehicle Model

As pointed out in chapter 1.4, the vehicle model forms the core of optimization methodology and is used to simulate the behavior of the testing vehicle. Depending on the desired accuracy and the area of investigation, there are many different types of vehicle models. A short excerpt based on [13] is presented in Table 2-1.

Table 2-1: Vehicle model types based on [13]

Model type	Degrees of freedom
Linear single-track model	2
Non-linear single-track model	3
Double-track model	4 – 30
Multi-body model	> 20
Finite-elements model	> 500
Hybrid model	> 500

The amount of degrees of freedom of a model is a measure for its complexity and considerably affects the expected computing effort.

Single-track models are suitable for basic investigations of the vehicle behavior. The front and the rear wheels are considered as only one wheel on each axle directly linked to the vehicle chassis. Here the lateral weight transfer during cornering is not taken into account.

The double-track model is a more complex model, which makes it possible to investigate lateral vehicle dynamics in a more accurate way. The linkage between wheels and chassis consists of springs and dampers. The kinematics of the suspension is simplified and modeled as pure vertical movement of the tire.

One of the objectives of this thesis is to investigate changes of suspension parameters which affect the kinematic behavior. Thus, a nonlinear three-dimensional multi-body vehicle model is used where all these effects are modeled. No elastokinematics are taken into account.

2.1 Multi-Body Vehicle Model

The vehicle model which forms the basis for all further investigations is intellectual property of Professor Georg Rill, from OTH Regensburg. Related explanations and detailed information about the model can be found in [14] and [15]. All equations and notations used in this chapter are based on these sources. The model is set up in MATLAB, which is primary used for numerical computations and is specializes in matrix manipulations and computations [16].

The model used consists of 9 individual entities; the chassis, four uprights and four wheels. An overview is depicted in Figure 2.1.

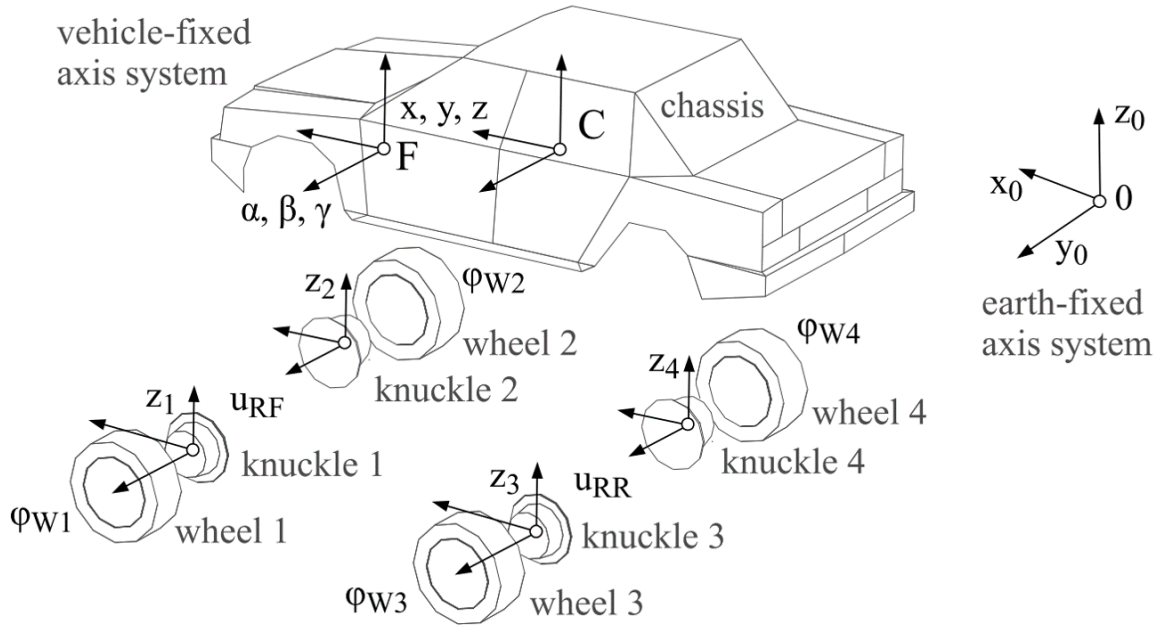

Figure 2.1: Multi-body vehicle model [14]

The location and the orientation of all these bodies can be fully determined by a set of generalized coordinates at any time. For each degree of freedom f, one coordinate is needed.

All variables related to the wheel positions are designated with indices from 1 to 4, standing for front left, front right, rear left and rear right.

2.1.1 Principle of Jourdain

In the multi-body vehicle model, all the bodies are connected with each other via links, joints and other guiding elements. The acting forces and torques on body i can be distinguished into two parts. Where for the forces can be written

$$F_{i,0} = F_{i,0}^{\mathrm{c}} + F_{i,0}^{\mathrm{a}} \tag{2.1}$$

and for the torques

$$T_{i,0} = T_{i,0}^{\mathrm{c}} + T_{i,0}^{\mathrm{a}} \,. \tag{2.2}$$

The first part declared with an c is related to the constraints and in the second part, all other acting forces, respectively moments, are summarized. It is possible to eliminate the resulting constraint forces, interacting between the bodies, to get a minimized set of differential equations.

Professor Georg Rill uses the principle of Jourdain in his model, which states that the virtual power of all constraint forces and torques occurring in the system must vanish. The equation for k bodies is written

$$\sum_{i=1}^{k} \left(\delta v_{0i,0}^{\mathrm{T}} \cdot F_{i,0}^{\mathrm{c}} + \delta \omega_{0i,0}^{\mathrm{T}} \cdot T_{i,0}^{\mathrm{c}} \right) = 0. \tag{2.3}$$

The constraint forces $F_{i,0}^{c}$ can be calculated from Newton's equation of motion

$$m_i \cdot a_{0i,0} = F_{i,0} \tag{2.4}$$

and respectively the constrain torques $T_{i,0}^{c}$ according to Euler

$$\theta_{i,0} \cdot \alpha_{0i,0} + \omega_{0i,0} \times \theta_{i,0} \cdot \omega_{0i,0} = T_{i,0} \ . \tag{2.5}$$

The virtual velocity $\delta v_{0i,0}$ and the virtual angular velocity $\delta \omega_{0i,0}$ of the body i are arbitrary and infinitely small.

2.1.2 Position and Orientation

The vehicle-fixed axis system is located on front axis of the car, in the middle of the centers of the wheels. The position in respect to the earth-fixed system is given by the vector

$$r_{0F,0} = \begin{bmatrix} x \\ y \\ z \end{bmatrix} \tag{2.6}$$

and the orientation by the rotation matrix

$$A_{0F,0} = \underbrace{\begin{bmatrix} \cos\gamma & -\sin\gamma & 0 \\ \sin\gamma & \cos\gamma & 0 \\ 0 & 0 & 1 \end{bmatrix}}_{A_\gamma} \underbrace{\begin{bmatrix} \cos\beta & 0 & \sin\beta \\ 0 & 1 & 0 \\ -\sin\beta & 0 & \cos\beta \end{bmatrix}}_{A_\beta} \underbrace{\begin{bmatrix} 1 & 0 & 0 \\ 0 & \cos\alpha & -\sin\alpha \\ 0 & \sin\alpha & \cos\alpha \end{bmatrix}}_{A_\alpha}. \tag{2.7}$$

Where α, β and γ are representing the roll, pitch, and yaw motion. It is assumed that the center of the wheel and the upright coincide. Thus, the positions of the wheel centers can be written as

$$r_{0i,0} = r_{0F,0} + A_{0F,0} \cdot r_{Fi,F} \ , \quad i = 1 \ldots 4 \, . \tag{2.8}$$

Steering rack position u and suspension movement z_i are input variables of the suspension model. A purely kinematical calculation returns the position and the orientation of the uprights relative to the vehicle-fixed axis system.

$$r_{Fi,F} = r_{Fi,F}(z_i \, , u_{\text{front}}) \, , \quad i = 1, 2 \tag{2.9}$$

$$r_{Fi,F} = r_{Fi,F}(z_i \, , u_{\text{rear}}) \, , \quad i = 3, 4 \tag{2.10}$$

The angles $\varphi_{\text{W}i}$ ($i = 1 \ldots 4$) designate the rotation of each wheel in respect to the upright.

2.1.3 Velocities

The absolute velocity of the vehicle-fixed axis system is calculated by

$$v_{0F,F} = \begin{bmatrix} v_x \\ v_y \\ v_z \end{bmatrix} = A_{0F}^{\mathrm{T}} \cdot \dot{r}_{0F,0} = A_{0F}^{\mathrm{T}} \cdot \begin{bmatrix} \dot{x} \\ \dot{y} \\ \dot{z} \end{bmatrix} \qquad (2.11)$$

And the absolute angular velocity is calculated by

$$\omega_{0F,F} = \begin{bmatrix} \dot{\alpha} \\ 0 \\ 0 \end{bmatrix} + A_{\alpha}^{\mathrm{T}} \cdot \left(\begin{bmatrix} 0 \\ \dot{\beta} \\ 0 \end{bmatrix} + A_{\beta}^{\mathrm{T}} \cdot \begin{bmatrix} 0 \\ 0 \\ \dot{\gamma} \end{bmatrix} \right). \qquad (2.12)$$

The velocity of each body i in respect to the earth-fixed axis system is given by deriving the position vector defined in equation (2.8)

$$v_{0i,0} = \frac{d}{dt} r_{0i,0}(y) = \dot{r}_{0i,0}(y)\,. \qquad (2.13)$$

These velocities are used as generalized velocities from now on.

2.1.4 Equations of motion

Using the principle of Jourdain leads to two first-order, inter-depending differential equations. The kinematical equation:

$$z = K(y) \cdot \dot{y} \qquad (2.14)$$

And the kinetical equation:

$$M(y) \cdot \dot{z} = q(y, z) \qquad (2.15)$$

The generalized coordinates are summarized in vector

$$y = [\ x,\ y,\ z,\ \alpha,\ \beta,\ \gamma,\ z_1,\ z_2,\ z_3,\ z_4,\ \varphi_{w1}, \varphi_{w2}, \varphi_{w3}, \varphi_{w4}\ ]^{\mathrm{T}} \qquad (2.16)$$

and the generalized velocities in vector

$$z = [\ v_x, v_y, v_z, \omega_x, \omega_y, \omega_z, \dot{z}_1,\ \dot{z}_2,\ \dot{z}_3,\ \dot{z}_4,\ \omega_1,\ \omega_2,\ \omega_3,\ \omega_4\ ]^{\mathrm{T}} \qquad (2.17)$$

$M(y)$ is the mass matrix with $f \times f$ elements, representing the masses and inertias as well as the partial velocities and partial angular velocities of the vehicle. It is defined by

$$M(y) = \sum_{i=1}^{k} \left(\frac{\partial v_{0i,0}^{\mathrm{T}}}{\partial z} m_i \frac{\partial v_{0i,0}}{\partial z} + \frac{\partial \omega_{0i,0}^{\mathrm{T}}}{\partial z} \theta_i \frac{\partial \omega_{0i,0}}{\partial z} \right) \tag{2.18}$$

for a system of k rigid bodies.

The $f \times 1$ vector $q(y,z)$ represents the generalized forces and combines the inertia and gyroscopic forces and torques with applied forces and torques and writes to

$$\begin{aligned} q(y,z) = \sum_{i=1}^{k} \Bigg(& \frac{\partial v_{0i,0}^{\mathrm{T}}}{\partial z} \left(F_{i,0}^{\mathrm{a}} - m_i a_{0i,0}^{\mathrm{R}} \right) \\ & + \frac{\partial \omega_{0i,0}^{\mathrm{T}}}{\partial z} \left(T_{i,0}^{\mathrm{a}} - \theta_{i,0} \alpha_{0i,0}^{\mathrm{R}} \right) - \omega_{0i,0} \times \theta_{i,0} \omega_{0i,0} \Bigg) . \end{aligned} \tag{2.19}$$

Where $a_{0i,0}^{R}$ and $\alpha_{0i,0}^{\mathrm{R}}$ are representing the remaining terms in the accelerations and can be written to

$$a_{0i,0}^{R} = \sum_{m=1}^{f} \frac{\partial v_{0i,0}(y,z)}{\partial y_m} \dot{y}_m \tag{2.20}$$

and to

$$\alpha_{0i,0}^{\mathrm{R}} = \sum_{m=1}^{f} \frac{\partial \omega_{0i,0}(y,z)}{\partial y_m} \dot{y}_m \, . \tag{2.21}$$

2.2 Steer-by-Torque Vectoring Model

The original vehicle model has 25 degrees of freedom. Steering rack position, braking and engine torques represent the driver inputs respectively steering, braking and accelerating.

To extend the original model (Chapter 2.1) for the purpose of SbTV investigation, it was adapted by Gerald Reiter in [17] who introduced one additional degree of freedom to enable SbTV simulations. The steering model is depicted in Figure 2.2.

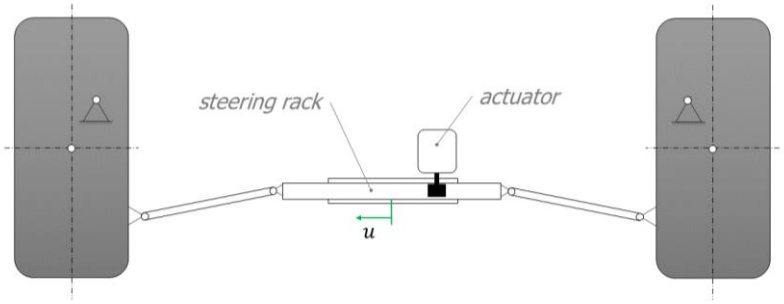

Figure 2.2: Steering system model based on [5]

To compute the steering rack position u, the following additional equation of motion was introduced.

$$M_u \cdot \ddot{u} = Q_u \qquad (2.22)$$

M_u represents the sum of reduced masses of the front wheels m_1 and m_2, the steering actuator and steering gear m_{red} and the steering rack m_{r}.

$$M_u = t_{1u}^{\mathrm{T}}\, m_1\, t_{1u} + d_{1u}^{\mathrm{T}}\, \Theta_1\, d_{1u} + t_{2u}^{\mathrm{T}}\, m_2\, t_{2u} + d_{2u}^{\mathrm{T}}\, \Theta_2\, d_{2u} + m_{\mathrm{r}} + m_{\mathrm{red}} \qquad (2.23)$$

Where t_{iu} stands for the partial derivation of the wheelcenter position to the rack position and is calculated by

$$t_{iu} = \frac{\partial r_{Fi,F}}{\partial u} \quad , \quad i = 1{,}2 \qquad (2.24)$$

and d_{iu}, the partial derivation of the wheelcenter rotation to the rack position, is written as

$$d_{iu} = \frac{\partial \varphi_{wi,F}}{\partial u} \quad , \quad i = 1{,}2\,. \qquad (2.25)$$

The force Q_u from equation (2.25) is given by

$$Q_u = t_{1u}^{\mathrm{T}} F_{1,C} t_{1u} + d_{1u}^{\mathrm{T}} T_{1,C} d_{1u} + t_{2u}^{\mathrm{T}} F_{2,C} t_{2u} + d_{2u}^{\mathrm{T}} T_{2,C} d_{2u} + \delta_u\, \dot{u} + F_{\mathrm{fr}}\,. \qquad (2.26)$$

Where $F_{1,C}$ and $F_{2,C}$ are the resulting tire forces on left and the right front wheel center. The resulting torques in respect to the wheel centers are labeled $T_{1,C}$ and $T_{2,C}$. F_{fr} represents the stick slip friction force and δ_u the friction coefficient.

2.3 Suspension Models

In the suspension models, all kinematical relations are defined and the positions of the uprights, and consequently of the wheels, are computed with respect to the vehicle-fixed axis system.

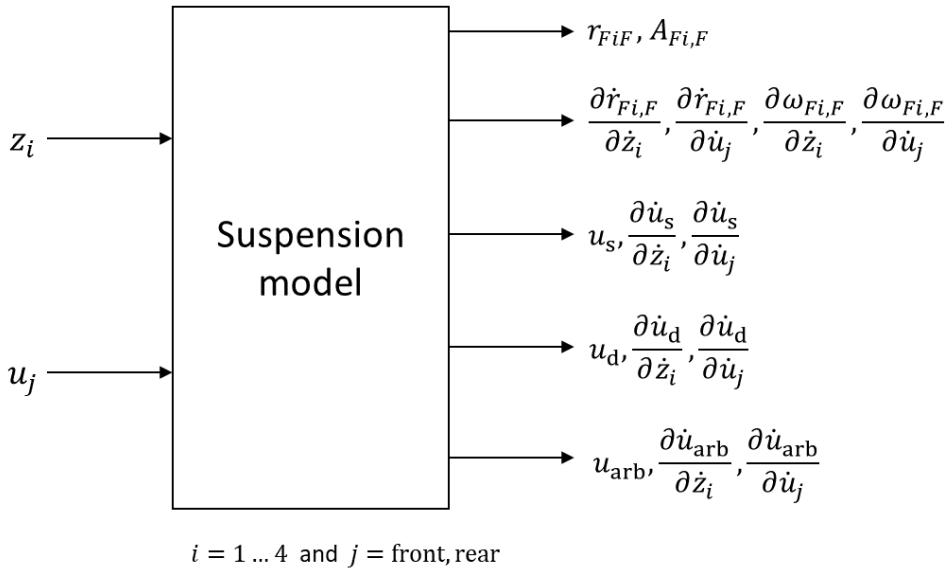

Figure 2.3: In- and output parameter of suspension models

Input parameters are the generalized coordinates z_i and u_j related to the corresponding corner of the car, where z represents the suspension position and u the position of the steering rack. As output the model provides the position $r_{Fi,F}$ and orientation $A_{Fi,F}$ of the uprights and additional all partial deviations in respect to the input parameters. Further the movement and partial derivation for all of the three force elements; spring, damper and anti-roll bar are calculated.

These values are used to compute the general forces and parts of the mass matrix declared in chapter 2.1.4.

3 Model Parametrization and Validation

3.1 Parameter Identification of Testing Vehicle

A parameter identification for the test vehicle described in 1.5 was carried out by Gerald Reiter in [17]. An excerpt of the validation methodology and the results is presented in this chapter.

The desired vehicle parameters are gathered from different sources, such as official reports and measurements executed by students.

To obtain the suspension kinematics behavior, the exact position of all hardpoints was determined by a three-dimensional measurement procedure.

The masses of the vehicle and its subsystems were weighted on scales. The position of the center of gravity of the whole vehicle was measured in lateral and longitudinal direction. The height above the ground was computed after weighting the vehicle in inclined position by measuring the occurring weight transfer with scales.

The moment of inertia tensors of specific bodies were calculated by using simple shaped substitution masses with consistent density. Additional for the whole vehicle the moment of inertia about the main axis was validated with data measured during specific test maneuvers.

3.2 Validation of Vehicle Model

To proof the correlation between model and test vehicle, the fully parametrized vehicle model was validated by comparison of measured data and simulation results. The validation was done in two steps. At first the conventional steering system was used and the basic vehicle behavior was validated. Afterwards the vehicle was steered with the SbTV system.

3.2.1 Validation of Conventionally Steered Vehicle

The road friction coefficient μ characterizes the grip level of the ground surface and is depending on weather conditions (wet and dry) and the type of tarmac. One task is, to adjust the coefficient used in TMeasy tire model to fit the simulation results to the recorded data.

The height of the center of gravity (h_{CoG}) of the vehicle has big influence on the load transfer and consequently on the vehicle behavior. Because of that and the possible measurement errors at the methodology used, h_{CoG} has to be tuned.

Thus, the first step of the validation process, was to adjust μ and h_{CoG} to obtain a good correlation. The basic steering behavior is compared in Figure 3.1. Further information concerning the steering behavior of a vehicle is given in Chapter 4.2. The right plot shows the achieved improvement in terms of correlation. To obtain this plots, the vehicle was moved in a corner with a constant radius of 60 meters.

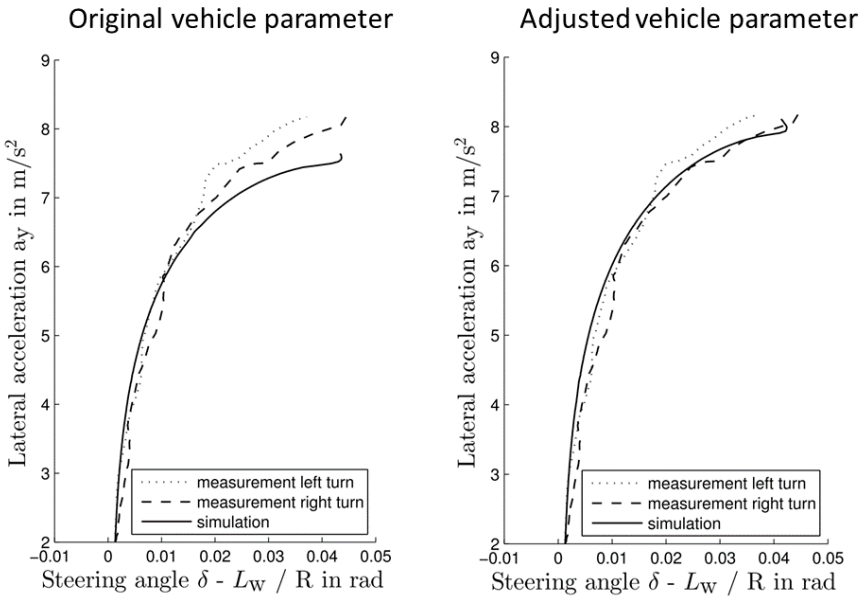

Figure 3.1: Steering behavior validation with conventional steering [17]

In the second step, dynamic driving maneuvers are used for validation purpose. In Figure 3.2 the lateral acceleration is plotted for a double lane change, a slalom and a step steer input at certain speeds.

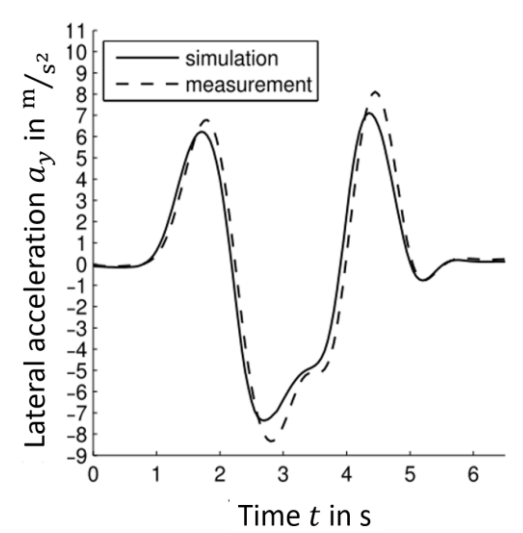

(a) Lateral acceleration for double lane change at 50 kph

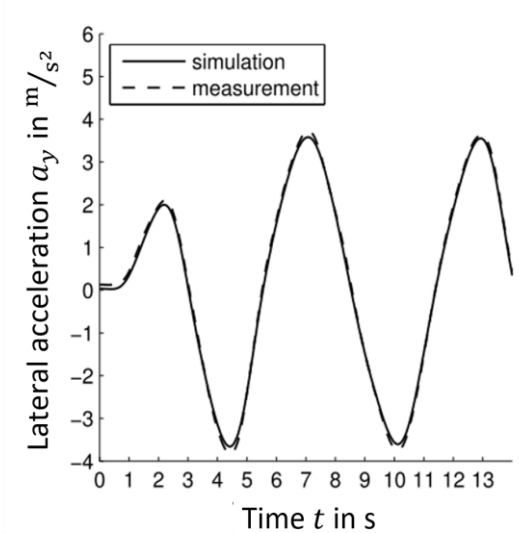

(b) Lateral acceleration for slalom at 70 kph

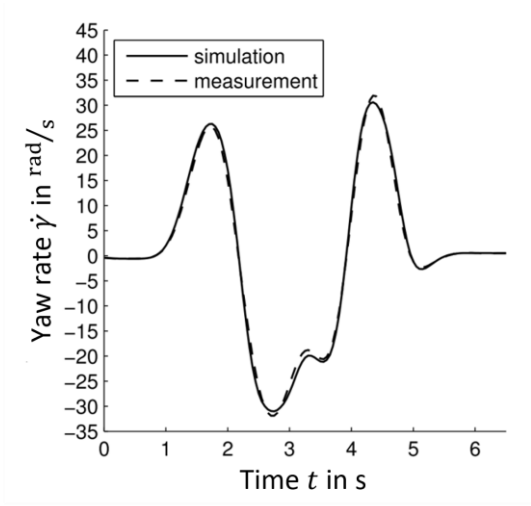

(c) Yaw rate for double lane change at 50 kph

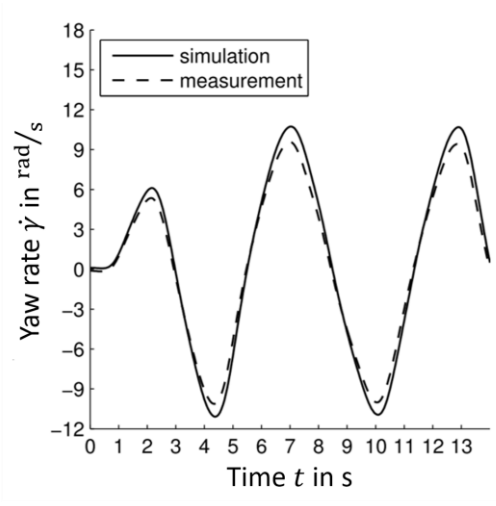

(d) Yaw rate for slalom at 70 kph

Figure 3.2: Vehicle model validation with different driving maneuvers [17]

Further investigations have been done for suspension movement, camber variation and yaw rate. Generally, a high level of correlation was achieved and therefore a good basis for the SbTV investigations was received.

3.2.2 Validation of Steer-by-Torque Vectoring

To validate the SbTV system, the lateral acceleration and the torque difference in relation to the steering rack position are investigated.

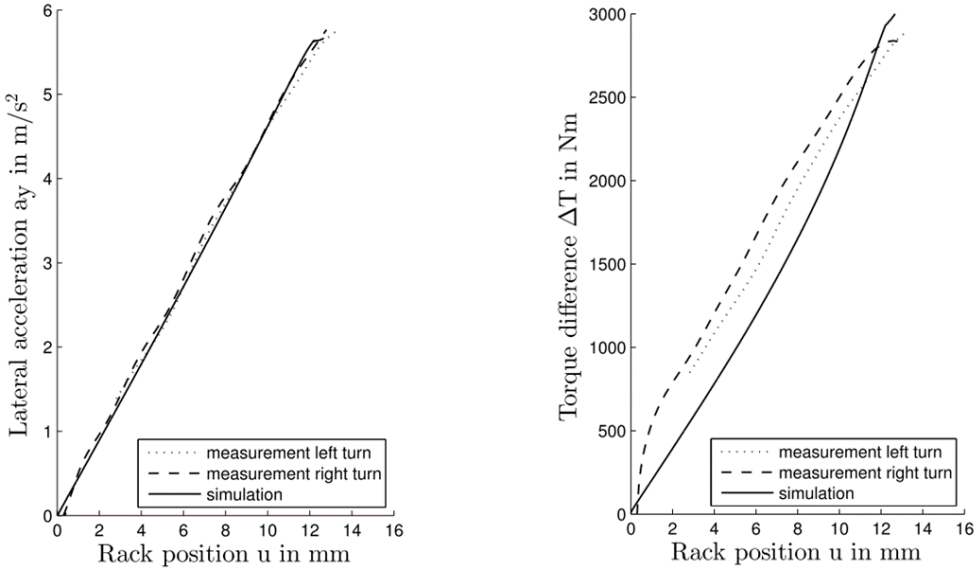

Figure 3.3: Steer-by-torque vectoring validation [17]

In the left plot, it is proven that the simulated lateral acceleration correlates quite well with the measurements thus the steering tendency is nearly identical. In the right plot, it can be noticed that the torque difference ΔT needed for a certain rack position in the simulation deviates from the measured values. This could be caused by the fact that a very simple rack friction model is used in the simulation or because the measured engine torques are actually estimated based on current measurement.

3.3 Parametrization of Tire Model

The tire model forms the mathematical expression of the interactions between the tire and the road [18] and computes all forces and torques acting on the tire. The operational properties of a road vehicle are highly affected by the behavior of the pneumatic tire [19]. Therefore substantial effort has to be put into the parametrization and validation of the model. According to [13], tire models can be divided into three main groups:

- Empirical models
- Physical models
- Semi-empirical models

3.3.1 TMeasy tire model

In the selected vehicle model, the TMeasy tire model, a semi-empirical model, is used [18]. This model also takes into account dynamic tire behavior. The dynamic reaction of the tire forces and torques is approximated with a first order system of differential equations [20].

All tire forces and torques are approximated by mathematical functions. The parametrization of the functions is done based on measured tire data, gathered from test-rig measurements.

3.3.2 Parametrization of the Tire Model

The tires used on the test vehicle were measured in Munich on the IABG test bench and the TMeasy tire model was parametrization based on this data by Klaus Esser [21]. Depicted in Figure 3.4 (b), (c) and (d) are the longitudinal force, the lateral force and the aligning torque of the tires. Each exemplary for three different vertical loads F_n.

(a) IABG test bench

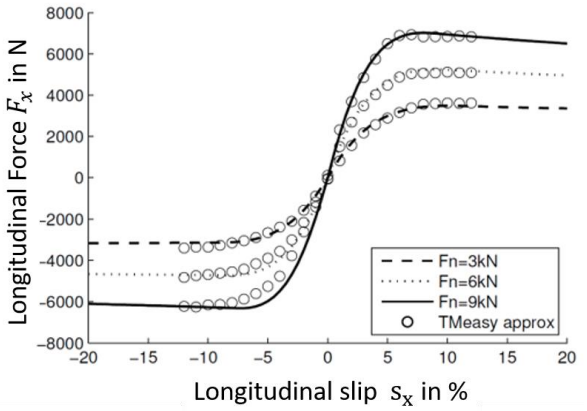

(b) Longitudinal force

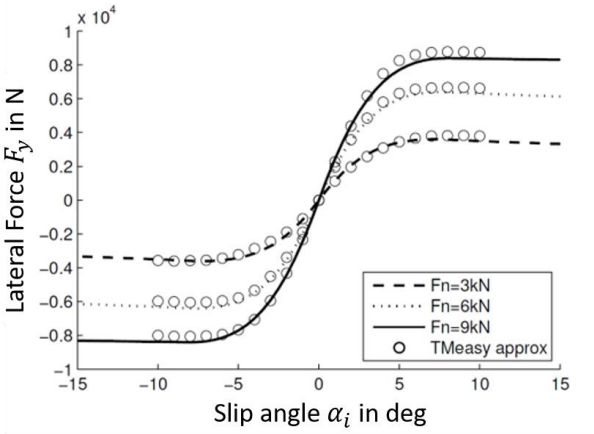

(c) Lateral force

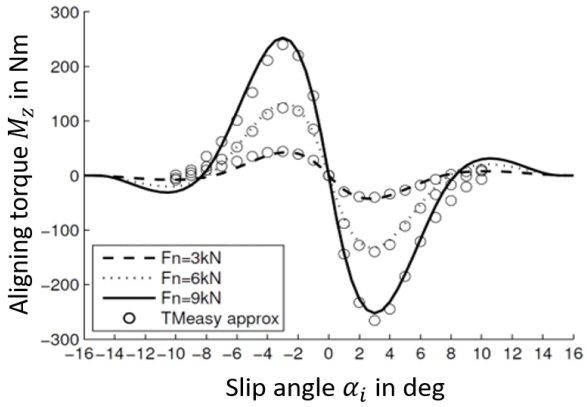

(d) Aligning torque

Figure 3.4: Tire data measurement and tire parametrization [21]

4 Objective Value Identification

As pointed out in chapter 1.3, a comparable value has to be found, which reflects the performance of the vehicle. The definition of performance in context with vehicle dynamics is not clearly defined in literature. In this thesis, it is associated to the horizontal forces acting on the car. This means if a vehicle is able to perform driving maneuvers at a high level of forces, respectively high accelerations, the performance is high. An additional criterium formulates the vehicle stability. Consequently, the performance of the vehicle is related to the tire utilization in a stable driving condition.

4.1 Vehicle Performance

As mentioned above the vehicle performance can be derived from the level of tire saturation the vehicle is able to achieve. This utilization can be investigated for one tire in Kamm's circle or the so-called friction ellipse.

4.1.1 The friction ellipse

The investigation of the forces acting on a tire is generally separated in longitudinal and lateral direction. The tire is able to transmit the maximal possible force in one direction, if the force in the other direction is equal to zero [22]. Depicted in Figure 4.1 is the friction-ellipse of a tire, representing the interaction of longitudinal and lateral forces at a certain tire load.

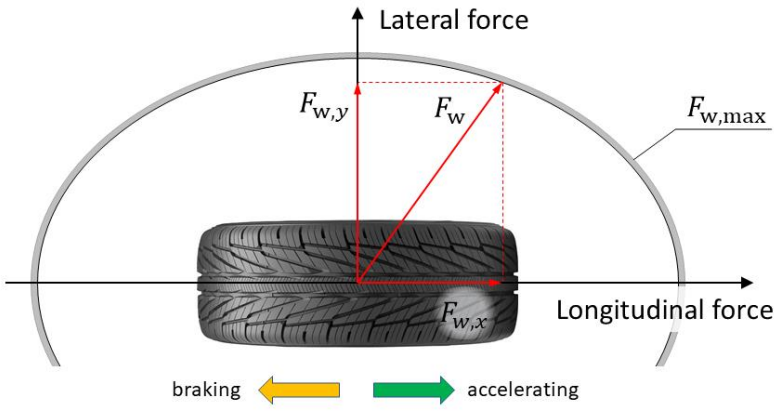

Figure 4.1: Tire friction ellipse based on [22]

The size and the shape of the ellipse changes with vertical tire fore and tire inclination which in turn are depending on the vehicle characteristics and driving condition.

4.1.2 The g-g Diagram and the Performance Envelope

Extending this consideration of one tire to the whole car, the vehicle performance can be visualized in the so-called g-g diagram, where the longitudinal acceleration of the vehicle is plotted versus the lateral acceleration. This plot has its origin in motorsport as a method of visualizing the performance of a racing car. The g-g diagrams are generally generated, based on measured data of a car driving around a race track as depicted in Figure 4.2.

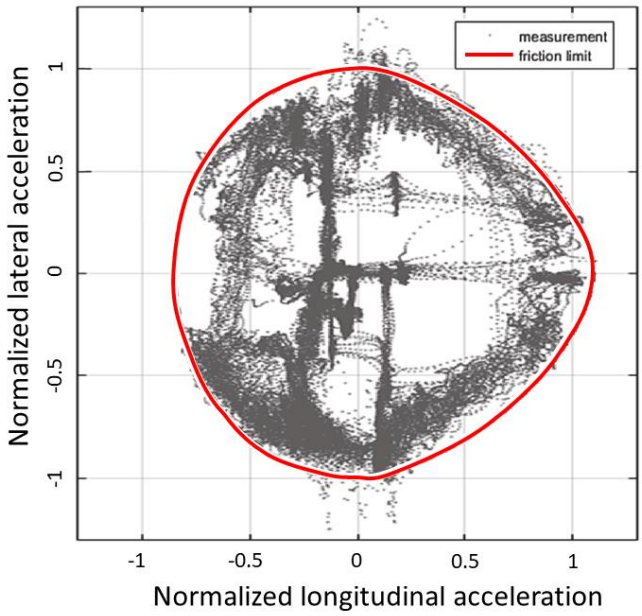

Figure 4.2: g-g diagram of vehicle measurements [23]

The theoretical acceleration limits can be estimated by drawing a line covering all feasible points. The target of a racecar, to achieve the minimum possible lap time, is reached if the vehicle is operated at this line [23].

This border can also be called the performance envelope (PE). It represents the ability of the car to exploit the tire forces driving on the limit and changes in size according to the vehicle performance. Therefore, the area of the PE writes to

$$PI = \int_{a_{x,\min}}^{a_{x,\max}} a_y(x) \cdot dx \qquad (4.1)$$

and is a good measure for the performance of the car.

It is solely depending on the road friction and on the vehicle velocity because of aerodynamic effects. It will be called performance index PI.

For the numerical computation of this border, model constraints are needed. To ensure that the calculated points on the PE are representing feasible and stable vehicle situation, a steady state condition is imposed. But because of the fact, that the longitudinal acceleration is not zero at most of these points, the calculated states are declared as “quasi-steady-state” (QSS).

4.1.3 The Yaw Moment Diagram

Another method developed by Milliken, the so called MRA Moment Method, also takes into account yaw acceleration of the vehicle [24]. This method investigates the stability and control measures in respect to certain steering and body-slip angles.

This diagram is not as suitable as the g-g plot for plain considerations in terms of vehicle dynamics performance because it is not possible to reduce the plot to a representative scalar value as done in 4.1.2. For that reason, it is not further investigated in this thesis.

4.2 Vehicle Handling

As mentioned above the g-g diagram can be used to investigate the vehicle performance, but no information can be given about the steering behavior experienced by the driver. For that reason, further investigations on the so-called handling of the vehicle have to be done. In the literature, the diagram depicted in Figure 4.3 is introduced for that purpose.

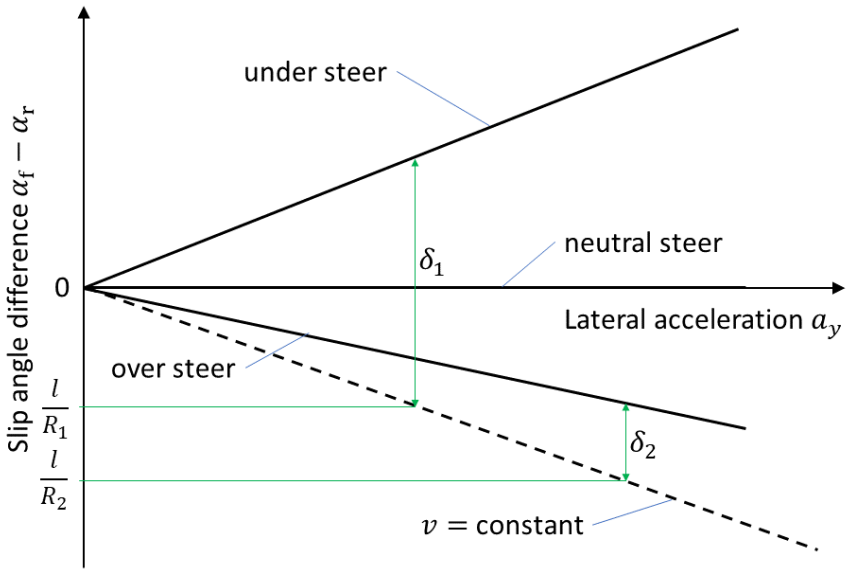

Figure 4.3: Steering characteristic based on [19]

Where α_f and α_r represent the slip angle on the front and on the rear axle of the car. In a double-track vehicle model it can be written for the tire slip angles of each tire α_1 to α_4

$$\alpha_\mathrm{f} = \frac{\alpha_1 + \alpha_2}{2} \text{ and } \alpha_\mathrm{r} = \frac{\alpha_3 + \alpha_4}{2}. \quad (4.2)$$

Further, the parameter l stands for the wheelbase of the vehicle and R for instant corner radius.

4.2.1 The Steering Index

The kinematic relation

$$\delta - (\alpha_\mathrm{f} - \alpha_\mathrm{r}) = \frac{l}{R} \quad (4.3)$$

can be deviated from the single-track model and it holds approximately for small angles. Where δ represents the steering angle of the wheel. The slip angle difference between front and rear axis can then be written as:

$$\alpha_\mathrm{f} - \alpha_\mathrm{r} = \delta - \frac{l}{R} \quad (4.4)$$

Plotting the slip angle difference versus the lateral acceleration gives an overview on the steering characteristic of the vehicle.

The slope of the steering characteristic can be calculated to

$$SI = \frac{\partial(\alpha_\mathrm{f} - \alpha_\mathrm{r})}{\partial(a_y)} \quad (4.5)$$

and gives a good indication of the behavior of the vehicle and is therefore also suitable to be used as objective value.

According to Figure 4.3 a vehicle has an understeering behavior if the slip angle on the front axle is increasing by a higher amount than on the rear axle in respect to a higher lateral acceleration. The steering index writes to

$$SI > 0 \quad (4.6)$$

for understeering behavior, and respectively

$$SI < 0 \quad (4.7)$$

for oversteering behavior of the vehicle.

4.2.2 Critical speed

Derived from Equation (4.3) the steering angle δ can be written as

$$\delta = (\alpha_{\mathrm{f}} - \alpha_{\mathrm{r}}) + \frac{l}{R}. \qquad (4.8)$$

In the linear region, the slip angle difference can be replaced with

$$(\alpha_{\mathrm{f}} - \alpha_{\mathrm{r}}) = \frac{v^2}{R} \cdot SI\,. \qquad (4.9)$$

and *(5.1)* can be rewritten to

$$\delta = \frac{v^2}{R} \cdot SI + \frac{l}{R}. \qquad (4.10)$$

It can be noticed that in the case of oversteering, δ changes the sign for a certain vehicle velocity v. The so-called critical speed can be determined based on [19] to

$$v_{\mathrm{crit}} = \sqrt{\frac{l}{-SI}}. \qquad (4.11)$$

The Equation (4.11) is valid only for oversteering. For understeering no instable point with rising speed is reached.

5 Performance Envelope Computation

The PE introduced in 4.1 is chosen as the basis of all further researches. It is assumed that the investigated vehicle is perfectly symmetric and the cornering performance in left and right corners is identical. Therefore, the PE will be calculated only for left hand corners. Further the aim in this thesis is to calculate solely points lying exactly on the envelope, this means computing the theoretical performance, the vehicle is able to achieve. The area of the PE defined in Equation (4.1) is representing the level of performance in terms of vehicle dynamics and is designated as performance index.

Using the PE as basis for vehicle dynamics ratings, is a novel approach and can not be found in the literature.

5.1 Quasi-Steady-State Condition (QSS)

The steady state condition in terms of vehicle dynamics designates an equilibrium of all forces and moments. This means there are no vehicle accelerations, beside the centrifugal acceleration. For the QSS a longitudinal acceleration is present and therefore the rotational wheel accelerations are also unequal to zero.

According to the notation introduced in 2.1 the following equations can be formulated.

5.1.1 Imposed Vehicle States

The calculation is done for a certain vehicle velocity v_{des}. It is imposed that the norm of the velocity vector equals

$$\text{norm}\begin{pmatrix} v_x \\ v_y \\ v_z \end{pmatrix} = v_{\text{des}} \,. \qquad (5.1)$$

Further the longitudinal vehicle acceleration $a_{x,\text{des}}$ is imposed with

$$a_x = a_{x,\text{des}} \,. \qquad (5.2)$$

The restriction for the rotational wheel acceleration $\dot{\Omega}_i$ for each wheel i can be formulated based on the definition of the longitudinal tire slip s_x in [14]

$$s_{x,i} = \frac{-(v_{x,i} - r_{\mathrm{D},i} \cdot \Omega_i)}{r_{\mathrm{D},i} \cdot |\Omega_i|} , \quad i = 1 \dots 4 . \tag{5.3}$$

With the assumption of very small changes of the slip and the dynamic tire radius $r_{D,i}$

$$\frac{ds_{x,i}}{dt} \ll 1 \text{ and } \frac{dr_{\mathrm{D},i}}{dt} \ll 1 \tag{5.4}$$

the relation between wheel rotational acceleration $\dot{\Omega}_i$ and the wheel slip can be written as

$$r_{\mathrm{D},i} \cdot \left(s_{x,i} \cdot \left|\dot{\Omega}_i\right| - \dot{\Omega}_i\right) + \dot{v}_{x,i} , \quad i = 1 \dots 4 . \tag{5.5}$$

Where $\dot{v}_{x,i}$ stands for the longitudinal tire acceleration.

5.1.2 Steady State Condition

All states equal to zero are summarized in the steady state conditions.

The time derivative of vertical distance of the vehicle-fixed axis system in respect to the earth-fixed axis system is given by

$$\dot{z} = 0 . \tag{5.6}$$

The angular velocities of the vehicle fixed axis system around the longitudinal and the lateral axis can also be set to zero. For the roll rate is written

$$\dot{\alpha} = 0 \tag{5.7}$$

and for the pitch rate

$$\dot{\beta} = 0 . \tag{5.8}$$

The suspension is not moving in the steady state condition with respect to the chassis and no damper forces are induced. Thus, the generalized suspension velocity

$$\dot{\varphi}_i = 0 , \quad i = 1 \dots 4 \tag{5.9}$$

must hold. Beside the gravitational acceleration g, no further acceleration in vertical direction occurs, so it can be written

$$a_z = 0. \tag{5.10}$$

Next all angular accelerations of the vehicle-fixed axis system with respect to the earth fixed system are determined. For the roll acceleration is written

$$\ddot{\alpha} = 0, \tag{5.11}$$

for the pitch acceleration

$$\ddot{\beta} = 0 \tag{5.12}$$

and at last for the yaw acceleration

$$\ddot{\gamma} = 0. \tag{5.13}$$

The acceleration of each suspension system is given by

$$\ddot{\varphi}_i = 0\,, \quad i = 1 \ldots 4\,. \tag{5.14}$$

As depicted in 2.2 the rack position u is introduced as additional vehicle state for the SbTV mode. Consequently, for investigations of this steering mode the equation for the steering rack acceleration

$$\ddot{u} = 0 \tag{5.15}$$

must hold. For investigations of the SbW mode equation (5.15) is not needed. The last equation and therefore the causes of the forces acting on the steering rack will be investigated in detail in 7.2.1.

5.2 Point Computation Methodology

The target of the algorithm is a fast and reliable calculation of the selected objective value. Before the area of the PE can be calculated a certain amount of discrete simulation points is needed. As mentioned in 5.1 at each point on the PE, the vehicle is in a QSS condition which can be described with a set of differential equations. Two solutions for this problem were identified:

5.2.1 Solve Equations

One consideration is, to impose longitudinal and lateral acceleration in all combinations in a certain range and try to solve the set of equations using an adequate algorithm. For a certain longitudinal acceleration, the slip angle on the front axle is increased step-by-step by which results in rising a_y. This is done until no higher lateral acceleration can be achieved. The methodology requires high computing power, because many points have to be calculated.

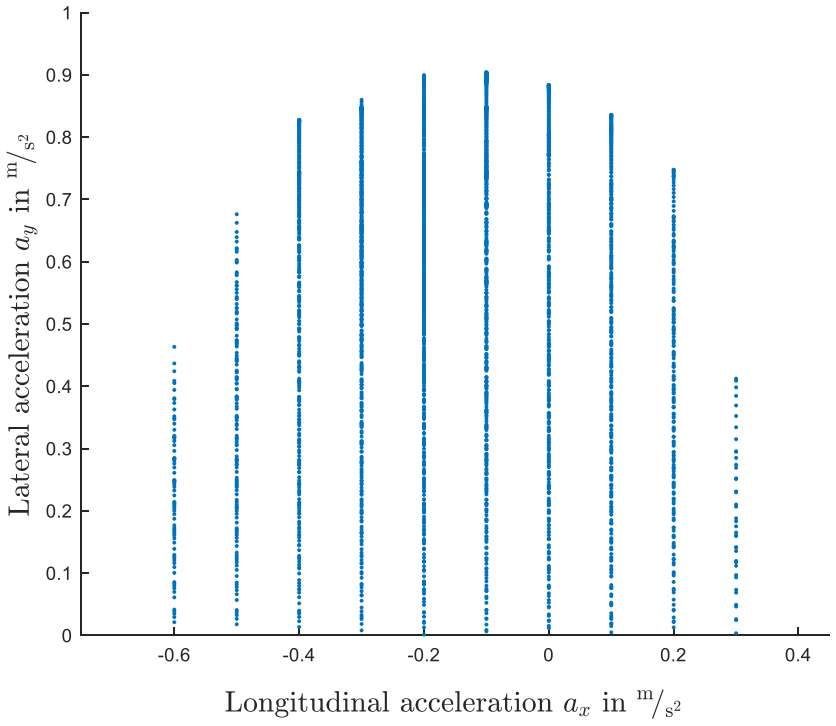

Figure 5.1: g-g plot point computation by solving equations

Depicted in Figure 5.1 is an example of this computation methodology. The idea leading to the next solution is, that a gradient-based optimization algorithm could be used to accelerate the computation of the points.

5.2.2 Constraint Optimization Technique

In this approach, an optimization algorithm is used to identify the points on the PE. The *fmincon*-function available in MATLAB for constrained, non-linear optimization problems is used [25].

Similar to the method introduced in 5.2.1 the points are determined for discrete longitudinal acceleration values. The target to reach the maximal lateral acceleration in respect to a specific longitudinal acceleration leads to a multi objective optimization problem. To compute the optimum of this type of problems two solutions are depicted in [11]:

- Weighting of objectives
- Fuzzy based decision-making scheme

To avoid the challenges coming along with this type of problems as the determination of feasible weighting-factors, it is possible to select one value as objective while imposing the other as constraint. With other words instead finding the optimum of

$$\max_{x \in \Re} f\left(a_x(x), a_y(x)\right) \tag{5.16}$$

with no constraints defined, it is tried to compute the optimum for

$$\max_{x \in \Re} f\left(a_y(x)\right), \tag{5.17}$$

subject to

$$a_x = a_{x,\mathrm{des}} \tag{5.18}$$

based on [11]. The rest of the constraints are formulated by the equations defined in 5.1, representing the QSS condition.

That means, beside the vehicle velocity, a certain longitudinal acceleration is imposed and the algorithm tries to maximize the associated lateral acceleration as visualized in Figure 5.2. The vehicle model computes all suspension kinematics and vehicle states and the optimizer is iterating until a specific stopping criteria is reached. The solution is feasible if no constraint has been violated. Compared to 5.2.1 less points have to be evaluated and the computation speed is increased.

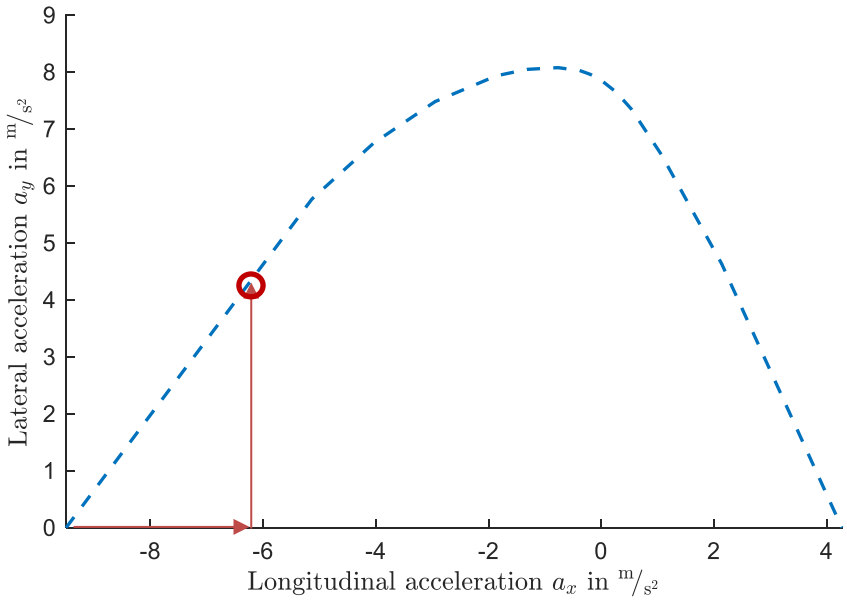

Figure 5.2: Performance Envelope

The solution is much quicker but it is necessary to observe the optimization algorithm in terms of stability and reliability. For example, the selection of “bad” starting conditions, results in non-feasible solutions, or in such, not representing global minima.

This leads to the computation strategy described below. The different points of the PE are calculated in a specific order so that more convenient starting conditions can be interpolated.

5.3 Vehicle Model Initialization

In the first step, the model initialization is done. A time-based simulation is started with an certain constant vehicle velocity and a certain initial position of the vehicle above the ground. A simple PI-controller is used to regulate the vehicle velocity and a steady state condition is reached after half a second as shown in Figure 5.3.

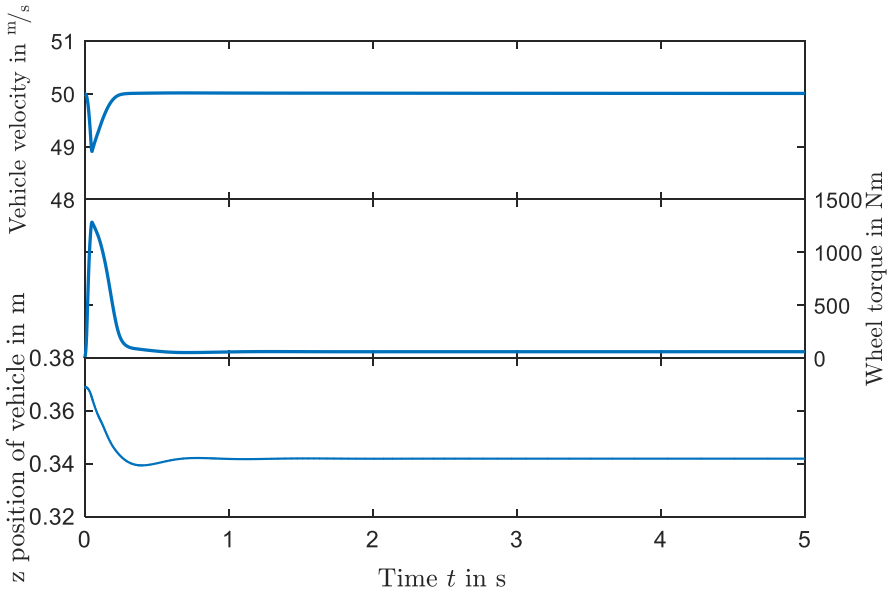

Figure 5.3: Vehicle state initialization

The initial values for the optimization algorithm are derived from the vehicle state reached at the end of the run.

5.4 Characteristic Points of the Performance Envelope

The intersections of the PE with the abscissa and the ordinate represent the performance of the vehicle in pure longitudinal, respectively in pure lateral direction. These points are selected as characteristic points and are calculated at the beginning.

The absolute minimum and maximum in longitudinal direction always coincide with the abscissa respectively with no lateral acceleration present. Contrary, the maximal lateral acceleration achievable can be at any point between the longitudinal limits. For that reason, the absolute maximum in lateral direction is also considered as characteristic point and calculated in the first step.

5.4.1 Lateral Acceleration Limit

This point represents the maximal lateral performance the vehicle can achieve. The corresponding longitudinal acceleration at this point is depending on vehicle specifications such as location of the driven axle, brake balance and the longitudinal position of the center of gravity.

For example, if a vehicle is designed to have an understeering behavior, it means that the tire saturation on the front axle is reached when the rear axle still has potential left. Braking adds more load to the front axle increasing the tire potential and therefore a higher lateral force can

be achieved. Too hard braking reduces the rear potential and the overall maximum is dropping again.

5.4.2 Longitudinal Acceleration Limits

The longitudinal acceleration limits are the maximum deceleration and the maximum acceleration the vehicle can achieve. It is assumed that the car is perfectly symmetric left to right and that the lateral acceleration is zero for these points.

In this case, the degrees of freedom of the model can be reduced. Consequently, the simulation speed and the system stability is increased. Thus additional equations can be formulated for the straight line behavior:

The roll angle and the yaw angle of the chassis become

$$\alpha = 0 \tag{5.19}$$

and

$$\gamma = 0\,. \tag{5.20}$$

Because of symmetric suspension load, it can be written

$$z_1 = z_2\,, z_3 = z_4\ . \tag{5.21}$$

Further the vehicle velocity in y-direction is given with

$$v_y = 0\,, \tag{5.22}$$

as well as the yaw rate

$$\omega_z = 0\,. \tag{5.23}$$

For the angular velocities of the wheels from the left and the right can be written

$$\Omega_1 = \Omega_2\,, \Omega_3 = \Omega_4\,. \tag{5.24}$$

5.4.3 Maximum in Lateral Direction at Zero Longitudinal Acceleration

For this point the longitudinal acceleration is zero and the maximum lateral acceleration for steady state cornering is obtained. Further this point is also needed if the steering behavior has to be computed.

No supplementary simplifications for the calculation can be made.

5.5 Additional Points for the Performance Envelope

Taking the points for maximum acceleration and deceleration in longitudinal direction, the space between can be divided in a certain amount of equidistant points. A fixed amount of this points is defined.

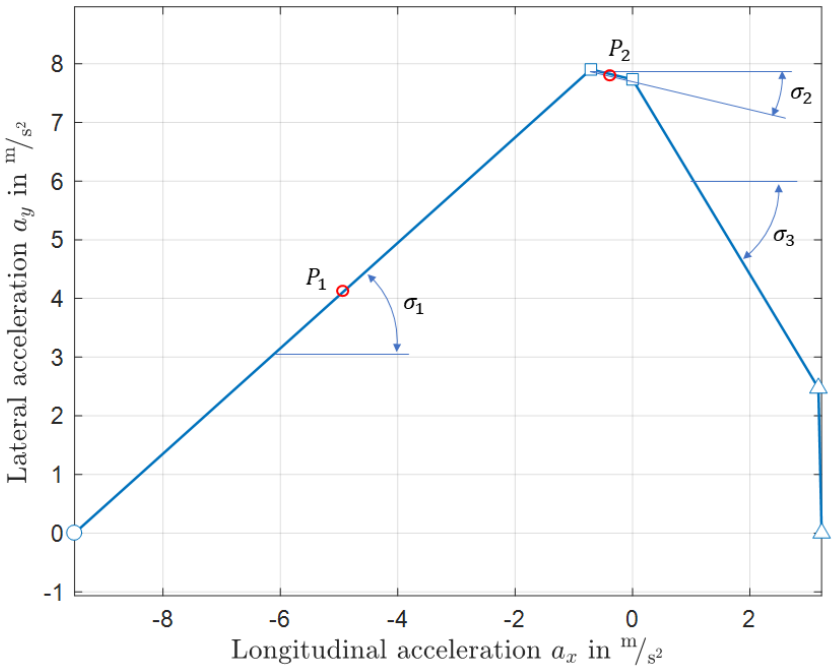

Figure 5.4: Additional points of the performance envelope

In the next step, the existing points are connected via straight lines as shown in Figure 5.4 and united to a preliminary PE. Then the slope of each section σ_1 to σ_n is determined and the differences between are evaluated. In regions with the highest slope deviations additional points are calculated. For the example shown the highest difference is between σ_1 and σ_2 and therefore in the next step the points P_1 and P_2 are computed. The procedure is carried out until one of the following conditions is reached:

- The value of maximal points allowed is surpassed.
- No slope difference beyond a certain value occurs.
- A specific value for the minimum distance to adjacent points is undercut

This leads to a smoothing effect applied to the PE and a minimum amount of points needed to draw the performance line in a sufficient way.

5.6 Border Criteria

The constraints for the optimization algorithm are defined by the equations representing the QSS condition. Additional constraints are introduced to tune the PE for special requirements.

5.6.1 Drivability Consideration

The calculation algorithm described above, computes the points of the PE not in behalf of drivability but considering the theoretical maximum achievable. To adapt the methodology for a human driver, additional constraints are defined.

It is assumed that the driver can not handle extensive values of lateral and longitudinal slip. Looking at the tire characteristic, slip values should be lower than the value related to the peak force. Further the permitted slip values on the rear axle should be lower than on the front. Depicted in Figure 5.5 are exemplary the restriction for the longitudinal slip.

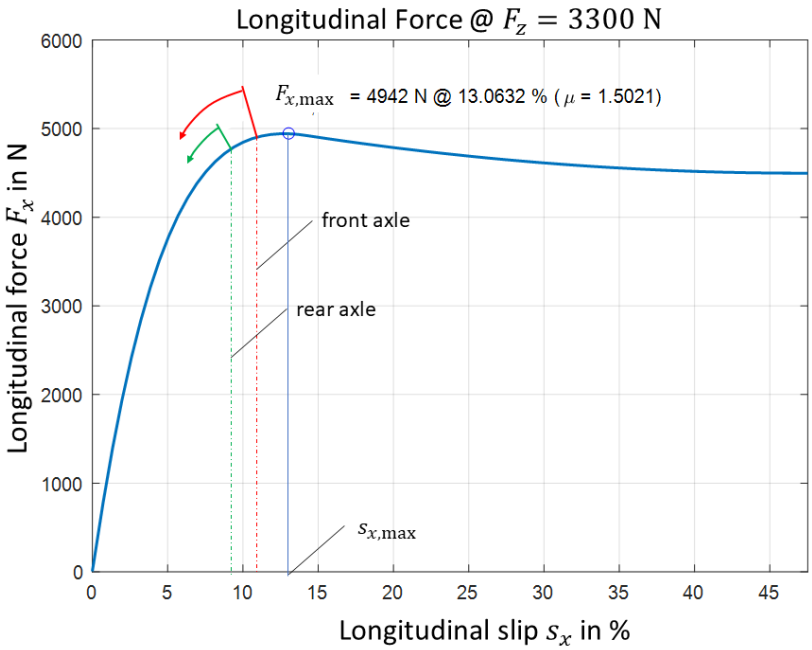

Figure 5.5: Longitudinal tire slip restriction

The constant limitation values $s_{xi,\lim}$ are chosen with respect to the equation

$$s_{xi,\lim} \leq s_{x,\max} \quad i = 1 \ldots 4 \qquad (5.25)$$

holding for all vertical tire loads F_z.

The limits for the lateral slip are identified in similar manor. The exact values of the introduced slip restrictions are based on experience of the company ThyssenKrupp Presta.

The impacts of using these additional constraints on the PE are shown in Figure 5.6 exemplary for the SbW system. The various kinds of shapes used for the points are representing different border criteria. Where $s_{x,i}$ for $i = 1 \ldots 4$ represents the longitudinal slip of tire i and respectively $s_{y,i}$ stands for the lateral slip.

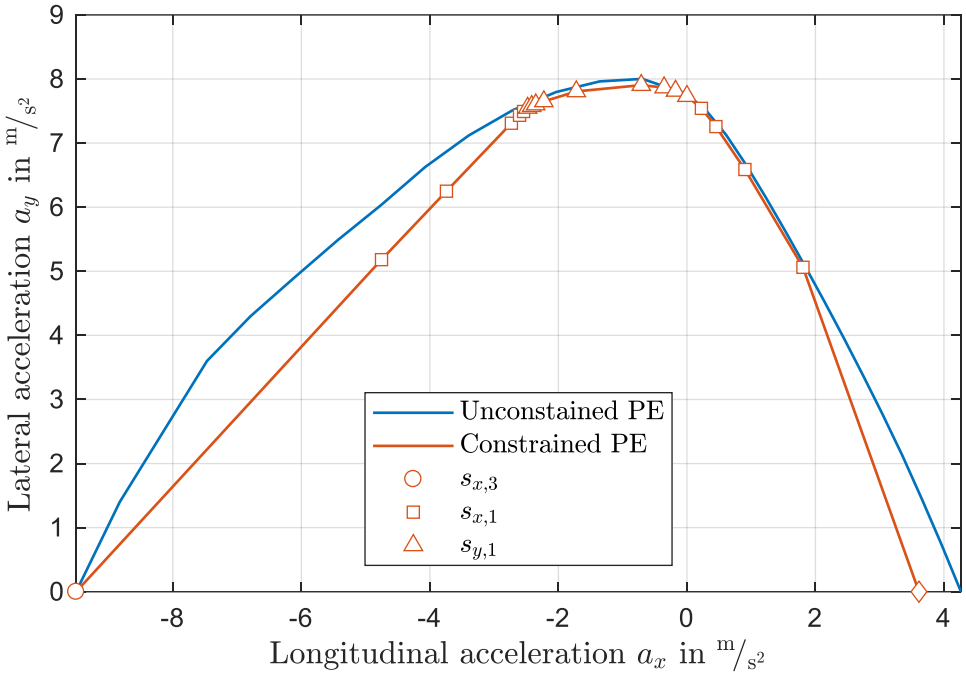

Figure 5.6: PE Border Restrictions

The point-related border criterion indicates which parameter is the responsible limiting-factor for the vehicle performance at this point.

5.6.2 Torque and Power Limitation

The torque and power limitation of the electric motors used on the testing vehicle have a huge effect on the acceleration-side of the PE which is depicted in Figure 5.7. The different shapes are related to the different border criteria shown in the legend. Where $s_{x,1}$ to $s_{x,4}$ represent the longitudinal slip of the tires and $s_{y,1}$ to $s_{y,4}$ respectively the lateral slip. T stands for the torque- and P for the power-limitation.

For a vehicle speed of 50 kph the blue curve shows that the limiting factor beyond a longitudinal acceleration of 3.2 m/s^2 is given by the maximum available torque and leads to an edge in the curve.

If the vehicle velocity 75 kph or higher, the limitation of the performance is given by the engine power. The yellow and the green line depict that the restriction results in a more smooth transition from the area of power limitation to the area of slip limitation.

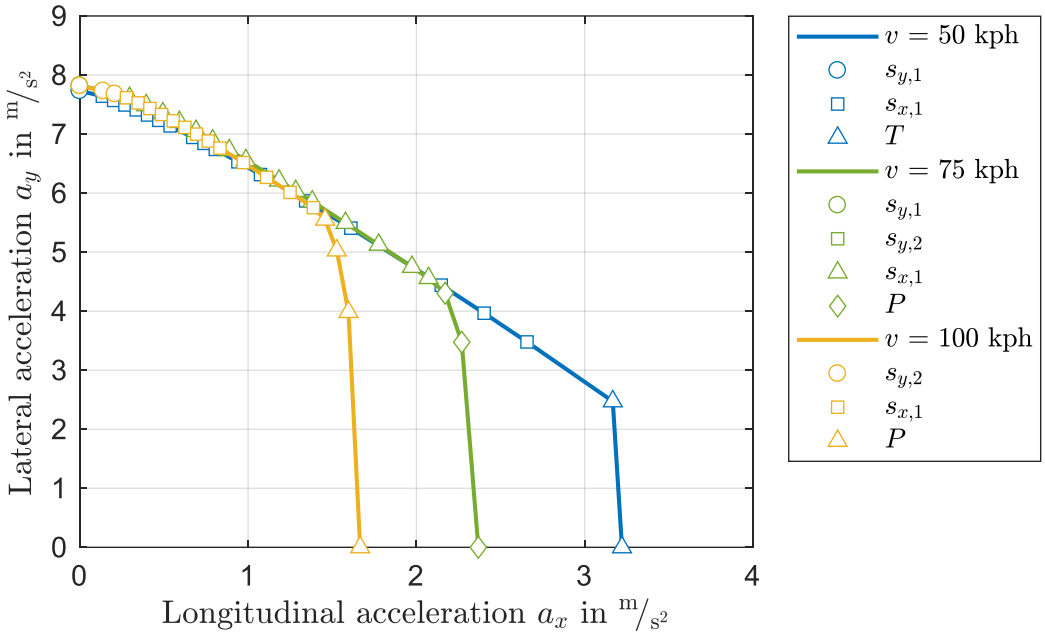

Figure 5.7: Torque and power limitation of the PE

The power limitation also influences the angular velocity of the driven wheels. Because of this a constant vehicle velocity of 50 kph is chosen for all further investigations to exclude the engine power from the limiting factors.

6 Steering Behavior Computation

Beside the performance index PI, the steering index SI defined in 4.2 can also be used as objective for the parameter optimization representing the steering characteristic of the vehicle. In terms of performance it is the goal to reach a high PI-value, but contrary for the SI it is not possible to identify an aspired optimum. This means there is no significance of a high or a low steering gradient. Consequently, it is more convenient to impose a desired steering characteristic SI_{des} and use it as additional constraint, which writes to

$$(SI - SI_{\mathrm{des}})^2 = 0 \qquad (6.1)$$

using a quadratic error function.

Then it is possible to optimize the suspension parameters of the testing vehicle to get the maximum vehicle performance for the SbTV mode, by imposing the same steering behavior as the vehicle in the SbW mode. This could be useful to adapt a suspension geometry of an existing SbW vehicle for the SbTV system, without changing the original vehicle behavior.

In this thesis, the steering behavior is used only for visual comparison perspectives. Because of the high grade of modification of the test vehicle, the computed SI-value for the SbW mode is considered to be not at its optimum and therefore not suitable as reference value.

6.1 Point Computation Methodology

The identical approach, as for the computation of the PE has been chosen to calculate a series of points representing the steering behavior in different conditions. That means by using an optimization algorithm the maximum possible lateral acceleration is calculated for a certain vehicle condition.

Depicted in Figure 6.1 is the steering characteristic of an understeering vehicle consisting of 10 different computation points.

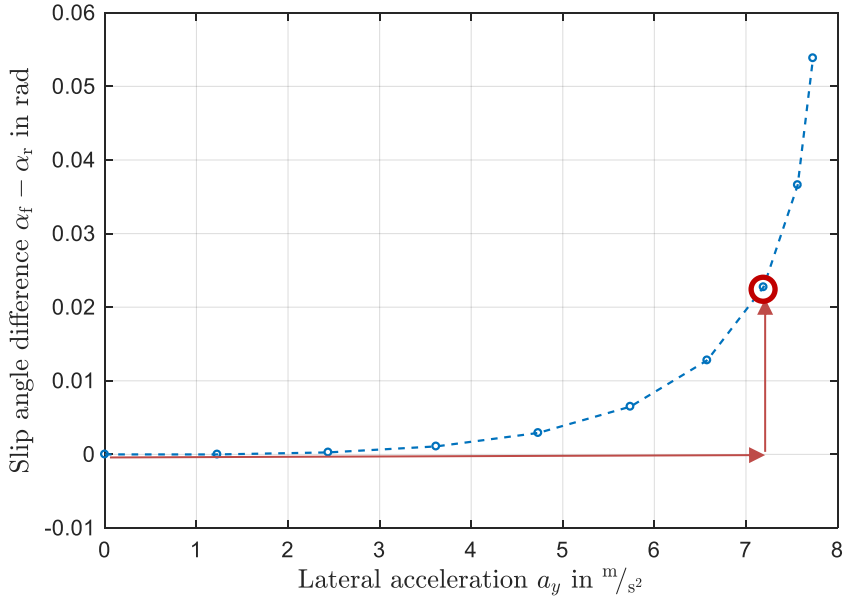

Figure 6.1: Steering index computation

6.2 Calculation Strategy

Contrary to the PE, the steering behavior is computed for the “real” steady state condition setting the longitudinal acceleration to

$$a_x = a_{x,\mathrm{des}} = 0 \qquad (6.2)$$

according to (5.2).

Additional to the imposed states declared in 5.1.1, the rack position is fixed for each desired point.

$$u = u_{\mathrm{des}} \qquad (6.3)$$

Corresponding to the PE, also characteristic points can be identified for the steering behavior. The first point is trivial, as at zero lateral acceleration no slip angle difference exists.

The end point is given by the point at the maximal lateral acceleration possible at no longitudinal acceleration. This point is also used for the computation of the PE, and defined in 5.4.3.

In the next step, the rack position occurring at the end point is taken as maximum rack position $u_{\max}$ and for the imposed rack position can be written

$$0 \leq u_{\text{des}} \leq u_{\max}. \qquad (6.4)$$

A certain amount of desired points is defined and a different desired rack position is assigned to each. After the computation of all points the slope of the linear range is computed after equation (4.5).

7 Parameter Optimization

The methodology developed in Chapter 5 formulates the basis for the parameter optimization. An arbitrary set of vehicle parameter can be selected to be optimized in respect to achieving the largest area under the PE, that means achieving the best vehicle performance.

To identify parameters with high influence on the vehicle performance a pre-evaluation is done and the sensitivity of the vehicle performance to certain parameters is analyzed.

7.1 Investigation of Initial Vehicle Conditions

In the first step, the initial conditions of the test vehicle are investigated. The vehicle operated in the SbW mode is compared with the vehicle steered by TV, leaving all vehicle parameters unchanged.

7.1.1 Initial Vehicle Performance

The vehicle performance of the different steering modes is depicted in Figure 7.1 and all border criteria are visualized. Where s_{xi} and s_{yi} represent the longitudinal and the lateral slip for the wheel 1 to 4. T stands for the torque limitation.

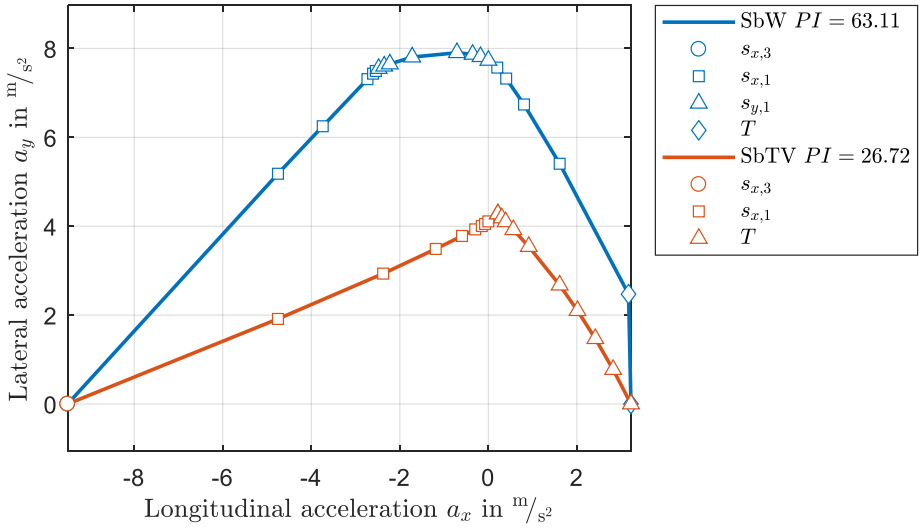

Figure 7.1: Performance Envelope for initial vehicle setup

It can be seen, that the performance loss is tremendous under the use of SbTV. The computed performance index PI, representing the area under the curve is reduced by nearly 58% compared to the SbW.

The performance on the accelerating side of the PE is mainly restricted by the maximal torque available. This is caused by the high demand of torque difference Δtrq for an imposed steering torque.

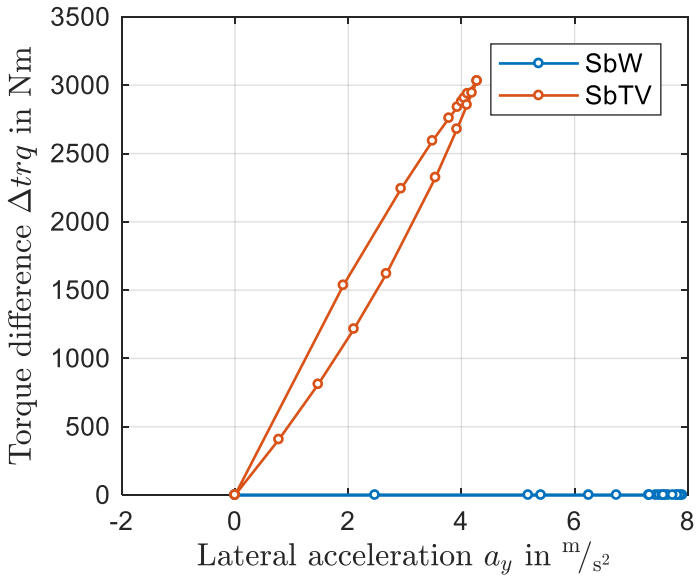

Figure 7.2: Torque difference demand for inital vehicle setup

The Δtrq demand, depicted in Figure 7.2 versus the lateral vehicle acceleration, forms a hysteresis. Where the lower limb corresponds to accelerating conditions and the upper to those under braking. The reason for this are the higher loads on the wheels in the front during braking which leads to higher horizontal forces and therefore a higher demand of imposed longitudinal steering forces.

7.1.2 Initial Steering behavior

Although the testing vehicle has been modified and the weight distribution has changed, in respect to initial vehicle, the steering behavior still is understeering as shown in Figure 7.3.

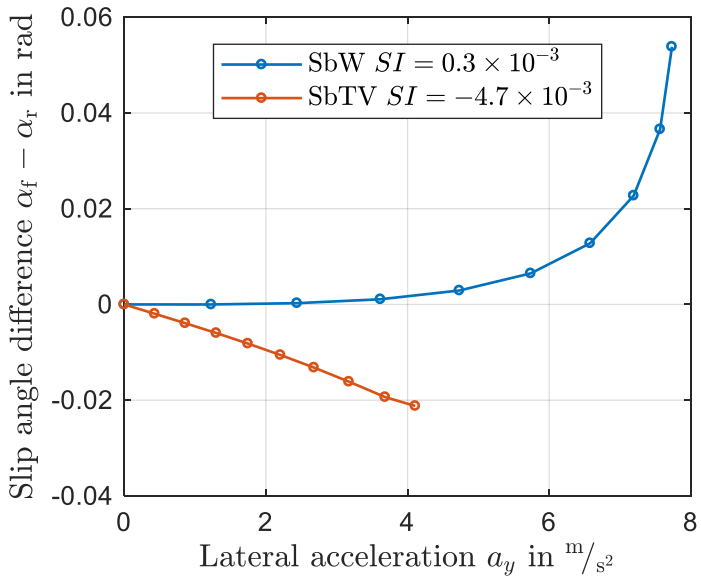

Figure 7.3: Steering behavior for initial vehicle setup

Contrary, the characteristic in the SbTV mode is oversteering and therefore possibly instable. The critical speed based on Equation (4.11) is calculated to 90 kph. That means the vehicle can get unstable above this velocity.

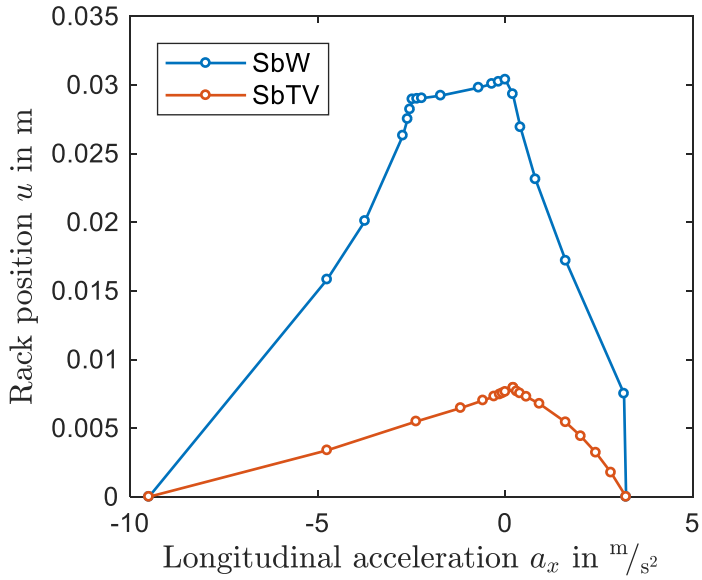

Figure 7.4: Rack position related to PE

In Figure 7.4, the rack position is plotted versus the longitudinal acceleration. It can be seen that for the SbTV mode the shape of the curve is similar to the PE. Contrary for the SbW, two edges occur dividing the curve into three lobes. These can be explained by looking at the border criteria in Figure 7.1, which show that the left and the right part are restricted by the longitudinal

slip on the front left tire $s_{x,1}$. Whereas the middle lobe is effected by the lateral slip on the front left tire $s_{y,1}$ and therefore the rack position is limited at these points.

Further it is shown that the absolute value of the rack position and consequently the steering angle of the wheels of the vehicle operated in the SbTV mode is much lower than using the SbW system. This is caused by the TV, which induces unequal longitudinal tire forces resulting in an additional yaw torque and an increase of the vehicle yaw rate. Therefore

7.2 Identification of Optimization Parameters

Theoretically all of the parameters, characterizing the vehicle model can be optimized for a certain objective. In this thesis only a few parameters are selected to demonstrate the functionality of the methodology.

7.2.1 Causes of Steering Torques

In addition to the short introduction of forces and dimensions effecting the SbTV performance for the 2D case in 1.2.2, a more detailed investigation of the suspension geometry of the steered axle is presented here.

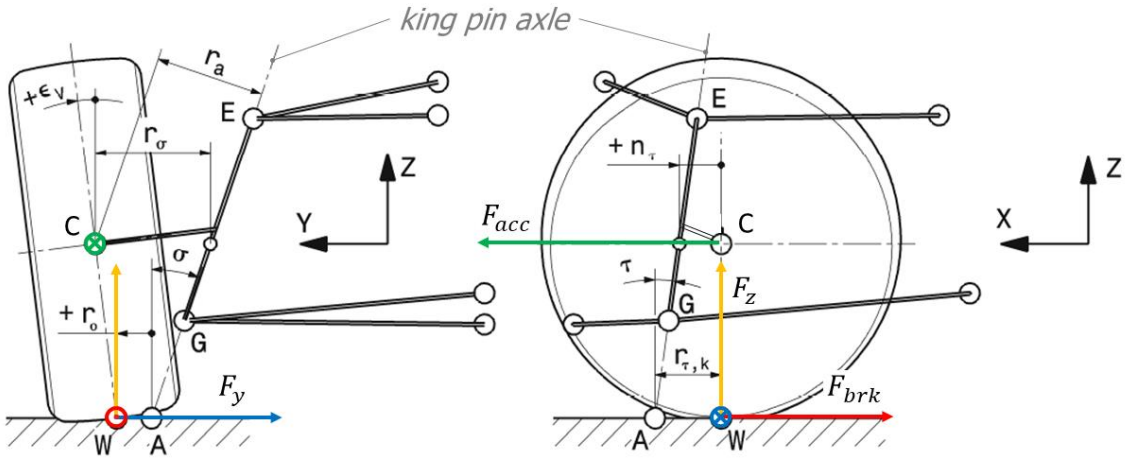

Figure 7.5: Forces and dimensions of a steering system based on [5]

Depicted in Figure 7.5 is a double-wishbone suspension where it is possible to give a good insight about the four possible causes of steering torques around the king pin axle.

The moment induced by lateral force F_y is calculated by

$$M_{lat} = F_y \cdot \left(r_{\tau,\mathrm{k}} + r_{\mathrm{P}}\right) \cdot \cos(\tau)\,, \qquad (7.1)$$

where $r_{\tau,\mathrm{k}}$ is the caster trail and r_{P} the pneumatic tire trail. The angle τ represents the caster angle.

Torques caused by the acceleration force are effected by the king pin offset r_a and can be written as

$$M_\mathrm{acc} = F_\mathrm{acc} \cdot r_\mathrm{a} \,. \tag{7.2}$$

Caused by the braking force F_brk and the scrub radius r_0 the related torque equals

$$M_\mathrm{brk} = F_\mathrm{brk} \cdot r_0 \cdot \frac{1}{\cos(\sigma)} \tag{7.3}$$

The angle σ denotes the so-called king pin inclination.

At last the torque induced by the vertical force F_z can be determined as function of 3D inclination of the king pin axle.

$$M_\mathrm{vrt} = M_\mathrm{vrt}(F_z, \sigma, \tau) \tag{7.4}$$

If the vehicle is steered with the TV in a stable condition, there has to be a torque equilibrium around the king pin axle. That means that the equation

$$\sum_{i=1}^{2} \left(M_{\mathrm{acc},i} + M_{\mathrm{lat},i} + M_{\mathrm{brk},i} + M_{\mathrm{vrt},i} + M_{\mathrm{r},i} \right) = 0 \tag{7.5}$$

must hold for the SbTV system. $M_{\mathrm{r},i}$ represents the torque induced by the steering rack force on wheel i. The equation (7.5) is equivalent to the in (5.15) defined steady state condition of the steering rack.

7.2.2 Steering Kinematics Evaluation

Based on the causes of the steering torque, introduced in 7.2.1, the main influencing parameters can be derived to:

- the caster trail r_P,
- the king pin offset r_a,
- the scrub radius r_0,
- the caster angle τ and
- the king pin inclination σ.

The dominant steering torques are induced by the lateral forces. For that reason, the caster trail is selected to be put under further investigations. Additional the scrub radius for braking conditions and the king pin offset for accelerating are determined to be the most influencing factors on the SbTV performance in conformity to [7] and [26].

7.2.3 Mechanical Vehicle Balance

The lateral weight transfer (WT) of a vehicle during cornering can be divided into 3 parts according to [27] as shown in Figure 7.6 exemplary for the front axle.

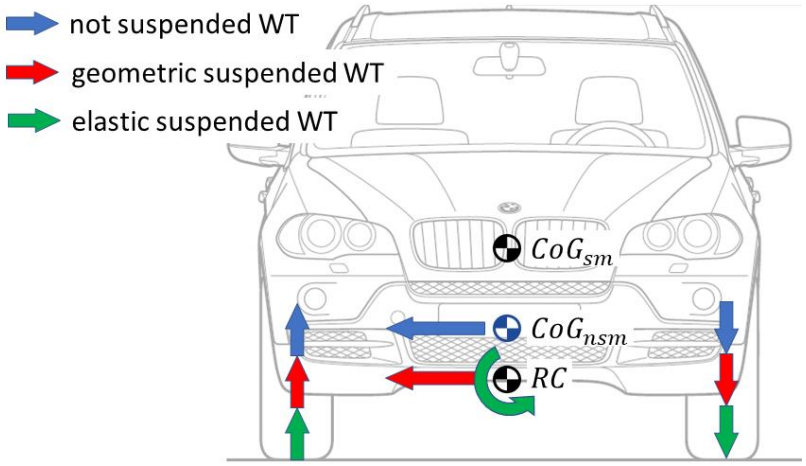

Figure 7.6: Lateral weight transfer during cornering based on [27] and [28]

The mechanical balance is defined as relation of front roll stiffness to the total roll stiffness.

$$MB = \frac{C_\mathrm{f}}{C_\mathrm{f} + C_\mathrm{r}} \tag{7.6}$$

The elastic WT is determined by the roll stiffness of the particular axle. By changing the anti-roll bar (ARB) stiffness or the spring stiffness the mechanical balance of the car can be influenced.

Because of the digressive behavior of the tires, the steering behavior of the vehicle can be changed by changing the mechanical balance, as reducing the weight transfer on one axle increases the lateral potential this axle and vice versa on the other axle.

Therefore, the front and the rear ARB stiffness is also investigated and a parameter optimization is executed.

7.3 Sensitivity to Road Friction

During a winter test on a snow-covered road with the BMW X5 it was shown that the performance difference of the vehicle in SbW mode versus the vehicle in SbTV mode is smaller than on normal tarmac.

Therefore, an investigation on the influence of the road friction coefficient on the performance has been carried out.

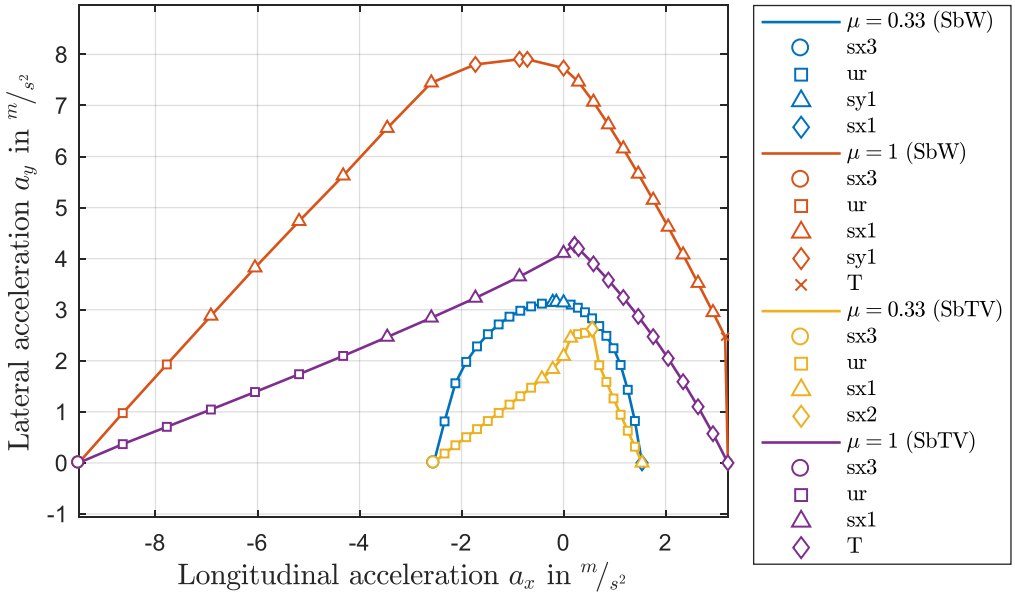

Figure 7.7: Performance envelope at different friction Levels

In Figure 7.7 is shown that the noticed effects during the test can be reproduced. For a road friction coefficient of $\mu = 0.33$ the SbTV performance losses are much lower than for $\mu = 1$.

Under normal circumstances on a dry asphalt, the SbTV performance is restricted by the maximum available torque or engine power. At low-friction conditions these limits can not be reached as the grip situation is too low. Therefore, the correlation of the vehicle performance gets better with decreasing road friction.

In Figure 7.8 it is shown that the steering behavior in linear region is not effected by the level of friction.

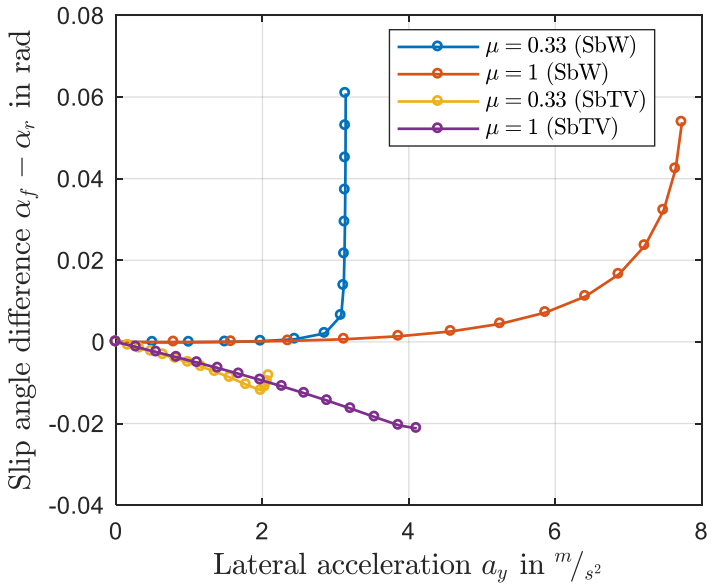

Figure 7.8: Steering behavior at different friction levels

8 Results

Because the focus of this thesis lies on the investigation of the torque vectoring applied during accelerating, only the right side of the PE is used for the performance investigations. Therefore, less points have to calculated which decreases the simulation time.

8.1 On Track Validation

Due to experiments with the test vehicle and preceding observations it was decided to modify the test vehicle. The design of the front axle suspension of the BMW X5 is depicted in Figure 8.1. On the left side, the original setup is shown. The intersection of the two black lines represents the virtual point of king pin axle which is the rotation axis in respect to the steering motion. The fact that the intersection point and therefore the king pin axle is very close to the wheel center plain, is problematical in terms of generating steering torques as explained in 7.2.1.

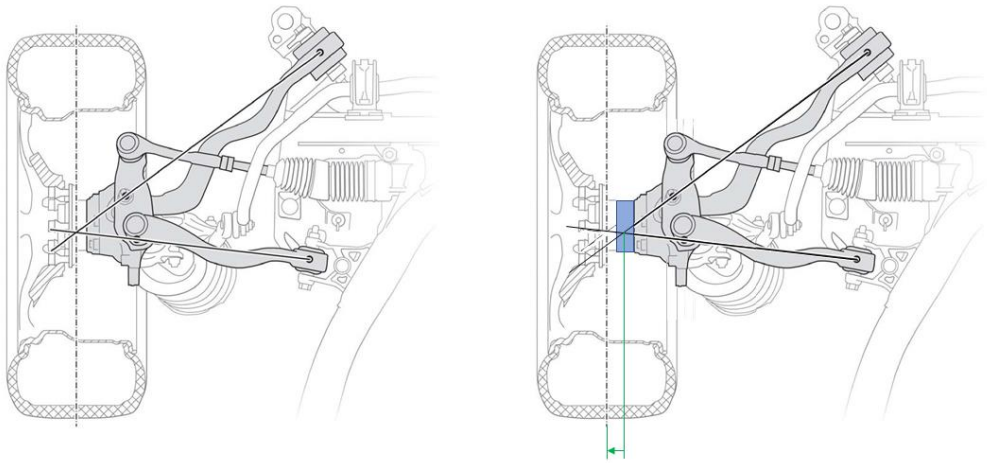

Figure 8.1: BMW X5 e70 front suspension geometry modification based on [29]

It leads to the approach of adding 35 mm spacer between the tires and the wheel hub to increase the lever of the induced longitudinal steering forces. The spacer width can not be chosen arbitrary, because of packaging reasons and the risk of a collision between the tire and the wheel house during steering.

In Figure 8.2 a comparison of measured data and simulated data of vehicle accelerations with the use of spacer and without is shown.

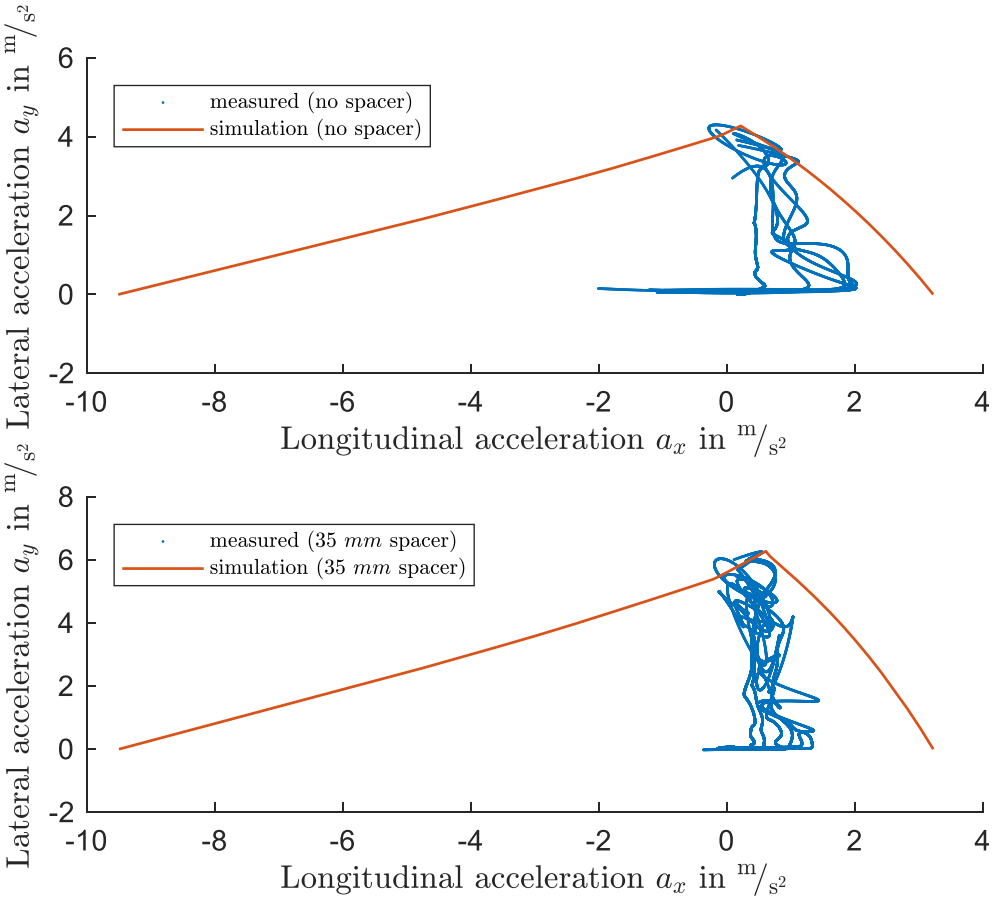

Figure 8.2: Correlation of simulation and measured data

The correlation of the measured data and the simulation is quite good which underlines the computed results. Because of the lack of measured data, the comparison can only be done for small values of longitudinal accelerations. It can be noticed, that with optimized suspension geometry, the vehicle performance can be improved. The maximal lateral acceleration increases from 4 to 6 m/s^2.

8.2 Optimized Steering Parameter

As defined in 7.2 the king pin offset and the caster trail are chosen as optimization parameters. The latter is variated by moving the wheel in longitudinal direction in respect to the wheel carrier. The optimization results are presented in Table 8-1 and the optimum values of both parameter are depicted.

Table 8-1: Values of optimized steering parameter

Parameter	Initial value	Optimized value
Movement of wheel in x-direction in mm	0	-5
Spacer width in mm	0	95

According to 8.1 the king pin offset is adjusted by using a spacer, moving the wheel in direction of the wheel axle. This is effecting also the track width of the vehicle and therefore the impacts on the PE are investigated.

8.2.1 Influence of Track Width Increase

To isolate the effect of increasing front track width the investigation is done with the SbW system. Depicted in Figure 8.3 are the effects of an increased track by 50 and by 100 mm. The symbols are related to the respective border criteria, where $s_{x,3}$ stands for the longitudinal slip at the rear left tire. Further $s_{x,1}$ and $s_{y,1}$ are the longitudinal and the lateral slip at the front left tire and T represents the torque limitation.

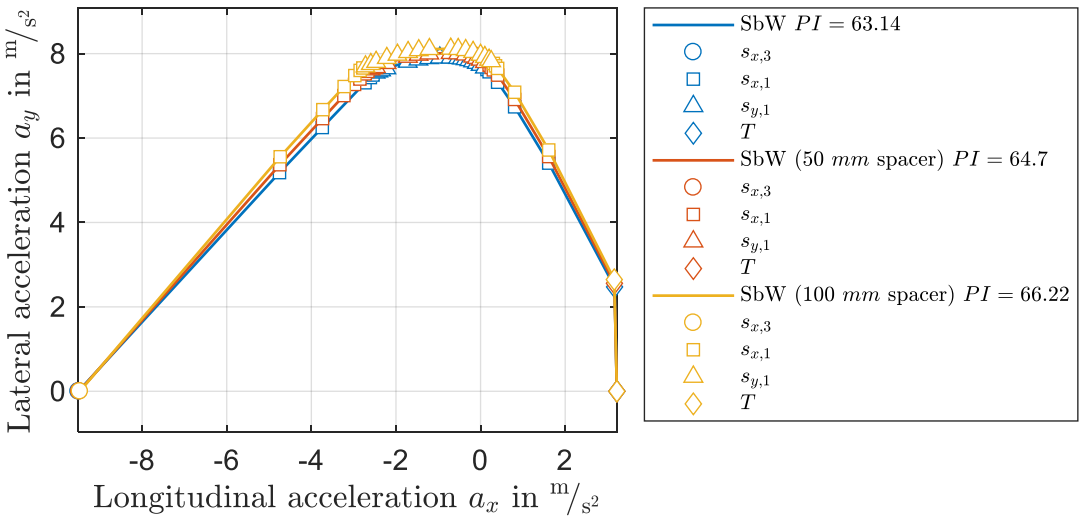

Figure 8.3: Front track width effects on performance envelope

The performance index increase is under 5%, which is acceptable for an 12% enlargement of the track width in case of the 100 mm spacer.

In Figure 8.4 it is shown that the effects on the steering behavior of the vehicle in the linear range are also very small.

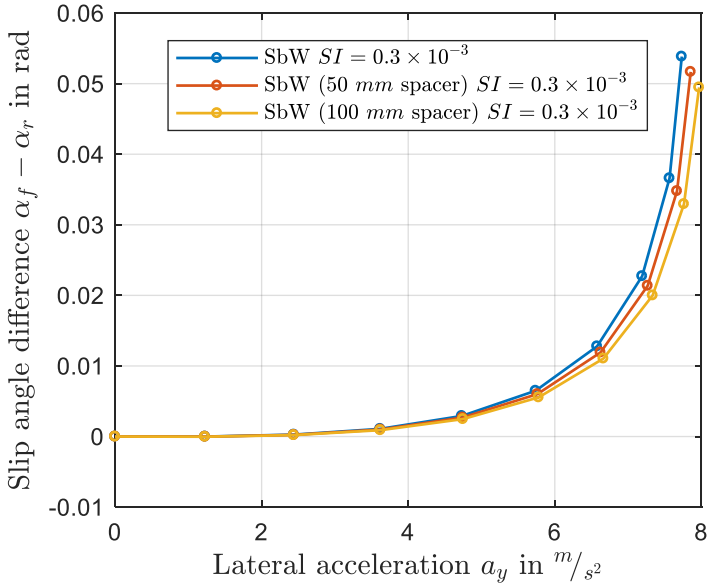

Figure 8.4: Front track width effects on steering behavior

8.2.2 Performance Gain due to Parameter Optimization

The achieved gain in vehicle performance using the optimized suspension parameters from Table 8-1 is substantial as depicted in Figure 8.5. As mentioned before only the acceleration side of the PE is shown. Again, the symbols are representing the different border criteria which were introduced for drivability reasons in 5.6. The longitudinal and the lateral slip are designated as s_{xi} and s_{yi} where $i = 1 \ldots 4$ refers to wheels of the car. T stands for the torque limitation.

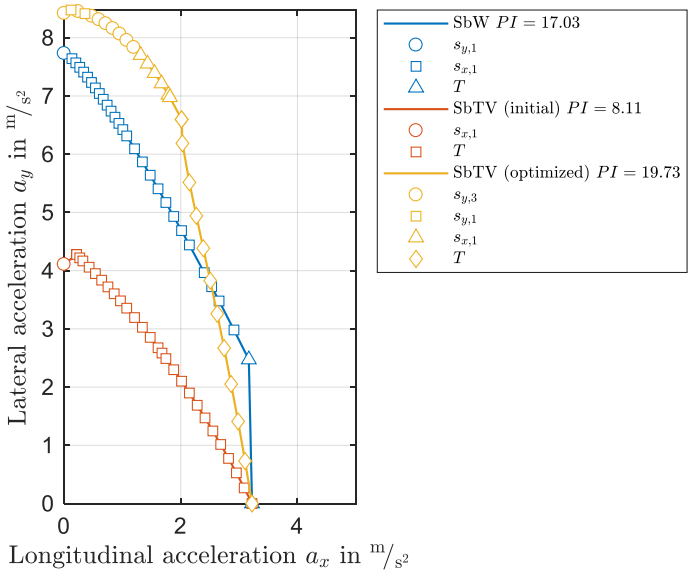

Figure 8.5: Performance of optimized steering parameters

The performance index is increased by over 140% in respect to the initial vehicle setup for the SbTV mode. It is even 15% better than the conventionally steered vehicle.

8.2.3 Steering Behavior due to Parameter Optimization

For the steering behavior of the vehicle shown in Figure 8.6, it can be said that for lower lateral acceleration values it gets less oversteer than the initial condition. After a certain value, where it becomes a neutral steering behavior, the car is understeering until it reaches the maximum.

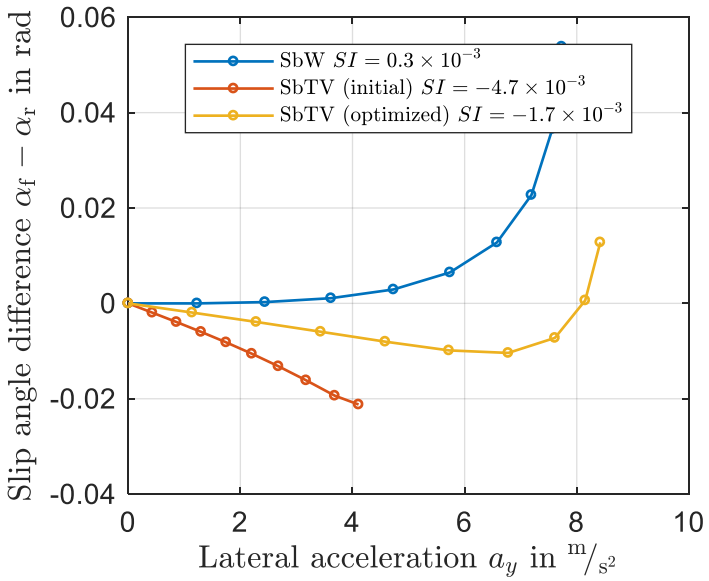

Figure 8.6: Steering behavior of optimized steering parameters

Comparing the slope of the curves in the linear region, it can be seen that the steering index is less than the half of the initial condition.

8.2.4 Steering torque demand due to Parameter Optimization

The demand of torque needed for the steering motion can be reduced tremendously, which is depicted in Figure 8.7.

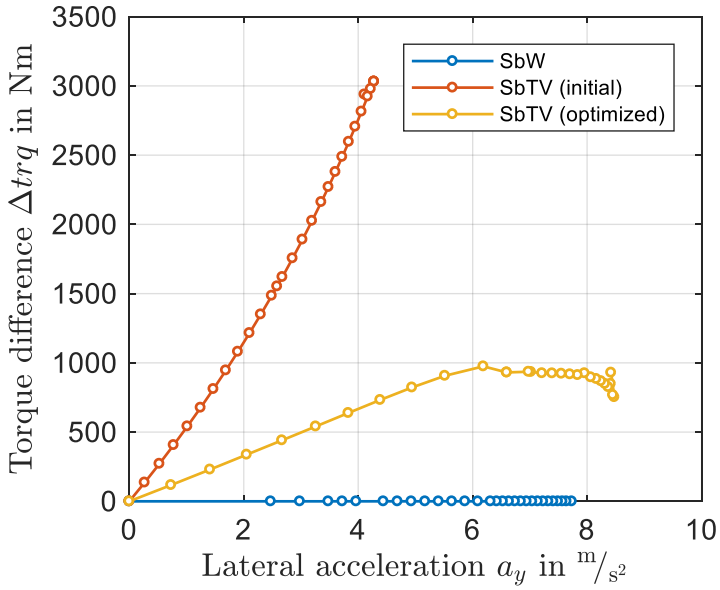

Figure 8.7: Torque difference of optimized steering parameters

The reduction of Δtrq was one of main targets and the assumption of an existing connection to the vehicle performance can be confirmed.

8.3 Optimized Mechanical Balance

Because the vehicle was modified and the weight and weight distribution changed, the idea is to re-balance the car by changing the mechanical balance as introduced in 7.2.3. This is realized by varying the front and the rear anti-roll bar (ARB) stiffness. The obtained results are shown in Table 8-2.

Table 8-2: Values of optimized ARB stiffness

Parameter	Initial value	Optimized value
Front anti-roll bar stiffness in N/m	28500	9060
Rear anti-roll bar stiffness in N/m	22700	9970

It can be noticed that the optimal values for the front and the rear stiffness are much lower than initial values. This could be caused by multiple effects. For example, the increased weight of the vehicle due to the modification leads to a higher compression of the springs. Therefore, at higher roll angles the bump stops could be hit. Because of the very high spring stiffness of the bump stop their contribution to the roll stiffness could outrange the effect of the ARB.

8.3.1 Performance Gain due to Re-Balancing

As shown in Figure 8.8 the effect on the PE by changing the roll-balance is much lower than the influence of the suspension parameters depicted in 8.2.

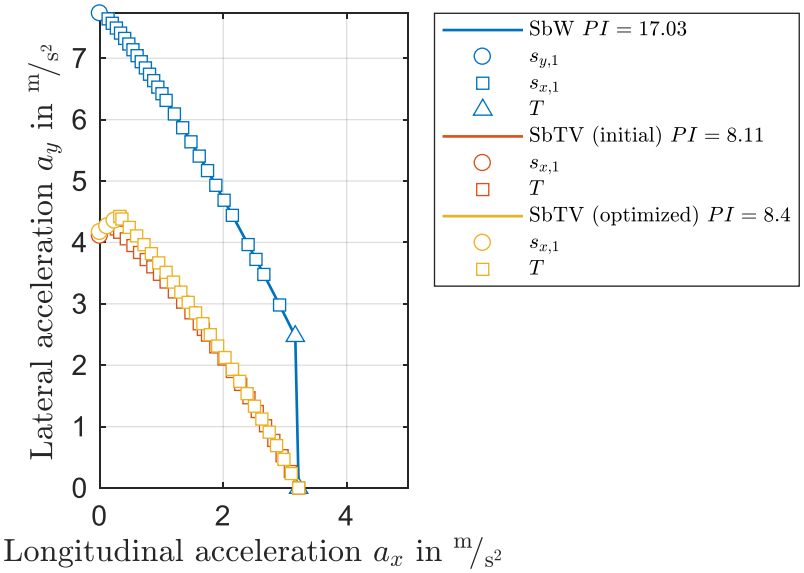

Figure 8.8: Performance of optimized ARB

Nevertheless, a small gain can be achieved and therefore the mechanical balance should be taken in account.

8.3.2 Steering Characteristic due to Re-Balancing

In terms of steering behavior for lower lateral acceleration values, almost no difference can be detected. In the region of higher values, the vehicle shows less oversteering, as shown in Figure 8.9.

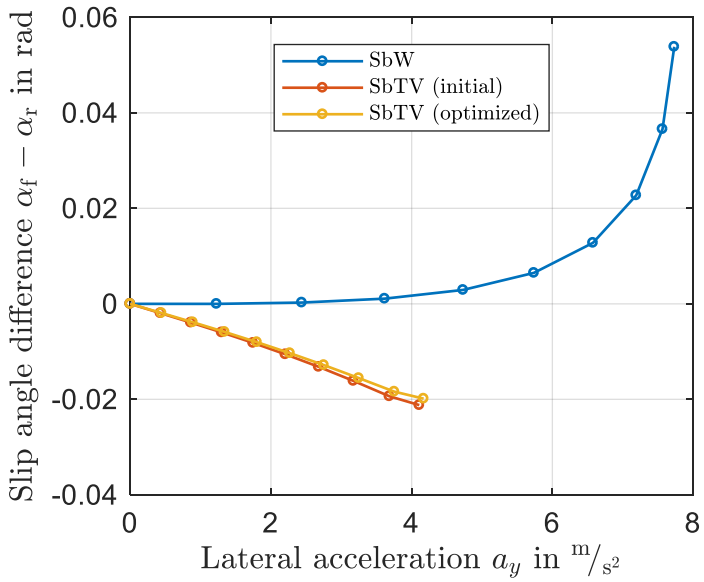

Figure 8.9: Steering behavior of optimized ARB

8.3.3 Steering torque demand due to Re-Balancing

As already shown above, the performance improvement is related to a reduction of the needed torque difference.

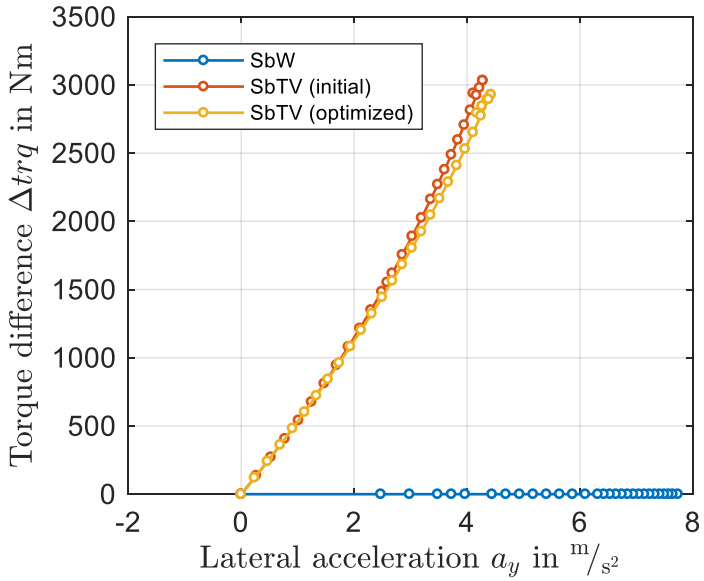

Figure 8.10: Torque difference of optimized ARB

So, the Δtrq desired to reach a lateral acceleration of $4\ \mathrm{m/s^2}$ can be reduced by approximately 200 Nm as shown in Figure 8.10.

8.4 Potential of Performance Improvement

The combination of SbW and SbTV is one possible application as defined in 1.3. Because of the expected possibilities using this combined steering system it is further investigated.

The distribution of steering force given by the driver and the force, resulting from SbTV, is determined by the optimization algorithm for each point. Depicted in Figure 8.11 for the combined steering mode it can be seen that the vehicle torque T is the limiting factor for high longitudinal accelerations from zero lateral acceleration up to beyond 8 m/s². The limitation for the maximum lateral acceleration is given by the lateral slip of the rear left tire s_{x3}.

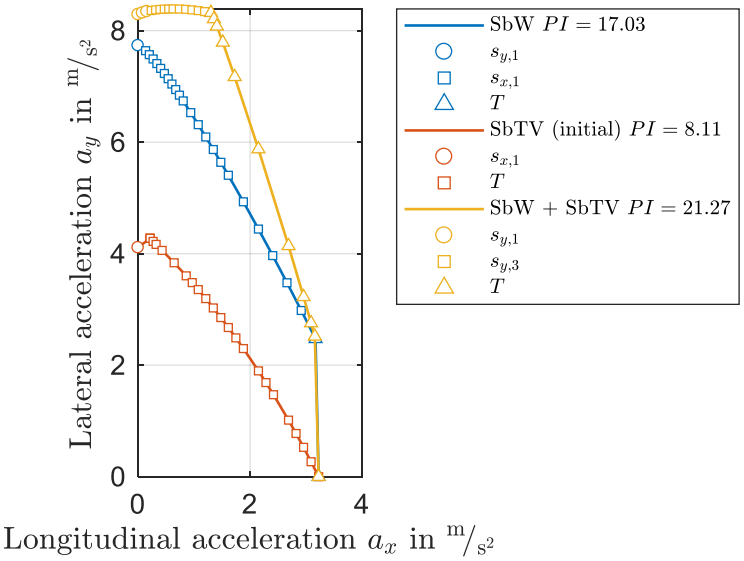

Figure 8.11: Performance potential of torque vectoring

It can be said that there is a remarkable performance gain caused by the usage of the combined steering system which is reached by the proper use of these two systems without changing one of the vehicle parameters.

9 Conclusion and Outlook

The goal of this thesis is the development of a computation methodology, which can be used for vehicle dynamics optimization. In particular the use of torque vectoring on the front axle to impose steering motions as an alternative to the SbW system were investigated and rated.

The vehicle model defined in Chapter 2 formulates the basis of all investigations. This model had been parametrized and validated in preceding works to connect the simulation results with a specifically adapted test vehicle build for the aim of testing novel steering systems.

Before the methodology could be set up, a representative value for the performance of the SbTV system was identified in Chapter 4. The performance envelope was introduced and its area was taken as measure for the performance level. All points formulating this envelope correspond to certain combinations of longitudinal and lateral acceleration values, representing the maximum horizontal force acting on the vehicle. It was defined that the vehicle condition is stable in all these points. Further, the steering characteristic was introduced to get insights into the vehicle behavior additional to its plain performance.

In the next step, a constraint optimization technique was chosen to compute the points of the performance envelope and the steering characteristic. The $fmincon$-function in MATLAB was used as computation algorithm. All equations representing the quasi steady state conditions were evolved and used as constraints for the optimizer. Additional restrictions were introduced in respect to the vehicle drivability.

The performance envelope computed by the methodology developed in Chapter 5 showed a dramatically performance loss for the SbTV system in respect to the conventional steering. Thus, the area under the performance envelope was used as objective value in a parameter optimization. At first it was shown that the performance can be increased tremendously by optimizing the steering geometry. In a second approach, the positive effects of finding the best roll-balance were successfully proven.

In conclusion, the developed methodology is capable of computing representative values and graphs for performance and steering of an arbitrary vehicle. Therefore, it can be used to find vehicle parameters which lead to the best vehicle performance. It is a very useful tool to study and develop novel steering systems, as it was intended.

The validation of the results gathered from the methodology has been done only for one parameter as the changeability of the test vehicle is limited. One possible next step would be to build

a fully adjustable research vehicle with SbW and SbTV systems on-board and use it in a loop with the computer software to develop new, advanced steering systems.

The methodology could also be easily extended to other steering, driving and braking mechanisms which could additionally improve the performance of a vehicle. An all-wheel drive system with four independent electric motors could be implemented to investigate all-wheel torque vectoring. Further a rear wheel steering system could be used and by adding one further degree of freedom as done in the front, the SbTV on the rear axle could be investigated. Steering the wheels with torques coming from power units is one possibility, but also a brake-by-wire system could be implemented to individually control the braking torques at all wheels. At last a combination of all mentioned techniques could be applied to the model, to get an idea of the potential within advanced steering systems.

List of Figures

List of Tables

Bibliography

[1] "ThyssenKrupp Presta AG," 19-Sep-2017. [Online]. Available: http://www.thyssenkrupp-presta.com. [Accessed: 24-Aug-2017].

[2] A. Franzen, "History of Steering," *prezi.com*, 05-May-2014. [Online]. Available: https://prezi.com/fqbtl8srz7cj/history-of-steering/. [Accessed: 20-Sep-2017].

[3] ThyssenKrupp Presta AG, "Steer-by-Wire," Essanestraße 10, Eschen, FL, Internal Documentation, 2016.

[4] P. Pfeffer and M. Harrer, *Lenkungshandbuch Lenksysteme, Lenkgefühl, Fahrdynamik von Kraftfahrzeugen*. Wiesbaden: Vieweg+Teubner Verlag / Springer Fachmedien Wiesbaden GmbH, Wiesbaden, 2011.

[5] W. Matschinsky, *Radführungen der Strassenfahrzeuge Kinematik, Elasto-Kinematik und Konstruktion*. Berlin: Springer, 2007.

[6] B. Heißing, M. Ersoy, and S. Gies, Eds., *Fahrwerkhandbuch*, 4., Überarb. und erg. Aufl. Wiesbaden: Springer Vieweg, 2013.

[7] K. Polmans, "Torque vectoring as redundant steering for automated driving or steer-by-wire," in *5th International Munich Chassis Symposium 2014*, P. E. Pfeffer, Ed. Wiesbaden: Springer Fachmedien Wiesbaden, 2014, pp. 163–177.

[8] M. A. Awan, "Compensation of low performance steering system using torque vectoring," PhD Thesis, Cranfield Univerity, 2014.

[9] J. Wang, Q. Wang, L. Jin, and C. Song, "Independent wheel torque control of 4WD electric vehicle for differential drive assisted steering," *Mechatronics*, vol. 21, no. 1, pp. 63–76, Feb. 2011.

[10] H. Benker, *Ingenieurmathematik kompakt - Problemlösungen mit MATLAB: Einstieg und Nachschlagewerk für Ingenieure und Naturwissenschaftler*. Berlin: Springer, 2010.

[11] U. Baumgartner, T. Ebner, and C. Magele, "Numerical Optimization," Technical University of Graz, Lecture Notes, 2010.

[12] M. Schneider, R. Vincenz, and A. Reichmuth, "SUNCAR Steer by Wire," ETH Zurich, Endbericht Mechanik und Thermomanagement, 2015.

[13] D. Schramm, M. Hiller, and R. Bardini, *Modellbildung und Simulation der Dynamik von Kraftfahrzeugen*, 2., Vollst. überarb. Aufl. Berlin: Springer Vieweg, 2013.

[14] G. Rill, *Road vehicle dynamics: fundamentals and modeling*. Boca Raton, FL: CRC Press, 2012.

[15] G. Rill, *Simulation von Kraftfahrzeugen*, 1994th ed. Braunschweig: Vieweg+Teubner Verlag, 1994.

[16] "MATLAB," *Wikipedia*, 04-Oct-2017. [Online]. Available: https://en.wikipedia.org/w/index.php?title=MATLAB&oldid=803726319. [Accessed: 14-Oct-2017].

[17] G. Reiter, "Basic Investigations and Parameter Identification of a Steer-by-Wire Torque Vectoring Vehicle," Master Thesis, University of Technology, Graz, 2016.

[18] W. Hirschberg, G. Rill, and H. Weinfurter, "User-appropriate tyre-modelling for vehicle dynamics in standard and limit situations," *Vehicle System Dynamics*, vol. 38, no. 2, pp. 103–125, 2002.

[19] H. Pacejka, TotalBoox, and TBX, *Tire and Vehicle Dynamics*. Elsevier Science, 2012.

[20] G. Rill, "First Order Tire Dynamics," in *III European Conference on Computational Mechanics: Solids, Structures and Coupled Problems in Engineering: Book of Abstracts*, C. A. Motasoares, J. A. C. Martins, H. C. Rodrigues, J. A. C. Ambrósio, C. A. B. Pina, C. M. Motasoares, E. B. R. Pereira, and J. Folgado, Eds. Dordrecht: Springer Netherlands, 2006, pp. 776–776.

[21] K. Esser, "Documentation IABG tyre measurement," ThyssenKrupp Presta AG, Report, 2016.

[22] M. Trzesniowski, *Rennwagentechnik: Grundlagen, Konstruktion, Komponenten, Systeme*, 4., Überarb. und erw. Aufl. Wiesbaden: Springer Vieweg, 2014.

[23] F. Goy, J. Wiedemann, T. Völkl, G. D. Colli, J. Neubeck, and W. Krantz, "Development of objective criteria to assess the vehicle performance utilized by the driver in near-limit handling conditions of racecars," in *16. Internationales Stuttgarter Symposium*, Springer, Wiesbaden, 2016, pp. 1213–1231.

[24] W. F. Milliken and D. L. Milliken, *Race car vehicle dynamics*. Warrendale, PA, U.S.A: SAE International, 1995.

[25] "Find minimum of constrained nonlinear multivariable function - MATLAB fmincon - MathWorks Deutschland," *mathworks.com*. [Online]. Available: https://de.mathworks.com/help/optim/ug/fmincon.html. [Accessed: 14-Oct-2017].

[26] M. Ryser, "Optimierung der lenkkinematischen Parameter für ein Elektrofahrzeug mit Einzelradantrieb," Bachelor Thesis, Swiss Federal Institute of Technology, Zurich, 2016.

[27] C. Rouelle, "Optimum G - vehicle dynamics solution," Cologne, Seminar handout, 2014.

[28] "Bmw X5 Blueprints Clipart," *Weclipart*. [Online]. Available: http://weclipart.com/gallery/bmw+x5+clipart/2. [Accessed: 21-Sep-2017].

[29] BMW, "Produktinformation Fahrwerk E70," BMW AG, User manual, 2006.